

Polarization dynamics in the paramagnet of a charged quark-gluon plasma

Lihua Dong^{✉*} and Shu Lin^{✉†}*School of Physics and Astronomy, Sun Yat-Sen University, Zhuhai 519082, China* (Received 21 March 2024; accepted 10 June 2024; published 9 July 2024)

It is commonly understood that the strong magnetic field produced in heavy ion collisions is short-lived. The electric conductivity of the quark-gluon plasma is unable to significantly extend the lifetime of the magnetic field. We propose an alternative scenario to achieve this: with finite baryon density and spin polarization by the initial magnetic field, the quark-gluon plasma behaves as a paramagnet, which may continue to polarize the quark after fading of the initial magnetic field. We confirm this picture by calculations in both quantum electrodynamics and quantum chromodynamics. In the former case, we find a splitting in the damping rates of probe fermions with an opposite spin component along the magnetic field. In the latter case, we find a similar splitting in damping rate of the probe quark in quark-gluon plasma in both high and low density limits. The splitting provides a way of polarizing strange quarks by the quark-gluon plasma paramagnet consisting of light quarks, which effectively extends the lifetime of the magnetic field in heavy ion collisions.

DOI: [10.1103/PhysRevD.110.016004](https://doi.org/10.1103/PhysRevD.110.016004)

I. INTRODUCTION

The observations of spin polarization in Λ -hyperons in heavy ion collision experiments have revealed quark-gluon plasma (QGP) as spin polarized matter [1]. The polarization is attributed to vorticity of QGP coming from initial orbital angular momentum in off-central collisions [2]. Theories based on spin-vorticity coupling have been developed in the past few years [3–7], giving satisfactory explanation of global spin polarization [8–12]. However, the spin-vorticity coupling alone predicts an equal polarization for both Λ and anti- Λ , while experiments have found splitting of polarizations for Λ and anti- Λ , with the splitting more prominent at low energy collisions. Different mechanisms have been proposed to understand the splitting, including spin-magnetic coupling [13–15], mean-field effect [16], direct flow effect [17], helicity vortical effect [18], etc.

While the mechanism of spin-magnetic coupling gives the correct sign of polarization splitting, it is generally expected that it cannot provide sufficient magnitude because the lifetime of the magnetic field is short so that the remaining magnetic field at freeze-out may be too weak. Indeed, recent studies suggest the magnetic field alone cannot explain the splitting at low energy [14,15]. The

evolution of the magnetic field has been studied using evolution of in-medium electromagnetic fields [19,20]. In order to have a long lifetime for the magnetic field, one needs to have large electric conductivity for the QGP medium, which is not favored by lattice studies [21–24]. Anisotropic conductivity in magnetized QGP has been considered in different approaches, including lattice [25], holography [26,27], and kinetic theories [28–35]. However, the situation does not improve significantly at phenomenologically relevant strength of the magnetic field. Other methods of constraining the strength of the magnetic field experimentally have been discussed in [36].

Most previous studies have treated QGP as a spinless fluid, which does not develop magnetization under an external magnetic field. Indeed, this is true for charge neutral QGP, in which the spin polarization due to spin-magnetic coupling cancels among positive and negative charge carriers. However, the cancellation is incomplete in a charged QGP, leading to nonvanishing magnetization. This is most clearly seen in the strong magnetic field limit, where the fermionic degrees of freedom are dominated by lowest Landau levels (LLLs), see Ref. [37] for a recent review. The magnetization by the LLL leads to net spin polarization in a charged QGP.¹ In particular, positively charged QGP relevant for heavy ion phenomenology corresponds to a paramagnet.

Recently, the magnetic susceptibility of charge neutral quantum chromodynamics (QCD) matter has been studied on the lattice in the weak magnetic field limit [38–40], see

¹QGP produced at low energy collisions has net baryon charge. It is also electrically charged for two-flavor QGP.

* Contact author: donglh6@mail2.sysu.edu.cn

† Contact author: linshu8@mail.sysu.edu.cn

Published by the American Physical Society under the terms of the Creative Commons Attribution 4.0 International license. Further distribution of this work must maintain attribution to the author(s) and the published article's title, journal citation, and DOI. Funded by SCOAP³.

also [41] for a study of charged QCD matter. The matter is found to be a paramagnet in the high temperature phase and a diamagnet in the low temperature phase. Here we consider instead charged QGP in the strong magnetic field limit. With net charge, we can loosely regard magnetization as spin polarization like in ordinary magnetic materials. The strong magnetic field limit is merely a technical simplification. With the apparent equivalence of magnetization and polarization in mind, we shall refer to charged QGP as a paramagnet² and explore its role in dynamics of spin polarization.

We will propose the following picture for magnetic field induced polarization dynamics in heavy ion collisions: while the magnetic field due to spectators in heavy ion collisions decays quickly, the strong magnetic field can convert the charged QGP consisting of light flavors into a paramagnet. The QGP paramagnet continues to polarize the strange quarks produced at a later stage in QGP evolution. The polarization is realized as a splitting of damping rates for strange quarks with opposite spin component along the magnetic field, which dynamically favors strange quarks with a negative spin component.

The paper is organized as follows: in Sec. II, we review photon self-energy in charged fluid consisting of LLL states and calculate the resummed photon propagator. We shall find an antisymmetric component unique to charged fluid, which is essential for polarization dynamics. In Sec. III, we consider a probe fermion in the paramagnet and find a splitting in the damping rates of the probe fermion with opposite spin component along the magnetic field. It provides a mechanism for polarizing the probe fermion. In Sec. IV, we extend the analysis to probe quarks in charged QGP. This case is complicated by the self-interaction of gluons, which gives rise to completely different dispersion of gluons. Nevertheless, we find the similar mechanism exists for probe quarks. We also discuss implications for heavy ion phenomenology. Section V is devoted to conclusions and a discussion of future directions.

We define $\epsilon^{0123} = +1$, $P^\mu = (p_0, \mathbf{p})$, $\sigma^\mu = (1, \boldsymbol{\sigma})$, and $\bar{\sigma}^\mu = (1, -\boldsymbol{\sigma})$.

II. PHOTON IN A PARAMAGNET

In this section, we study the dynamics of a photon in charged magnetized plasma. The case for charge neutral plasma has been studied extensively in literature, see Refs. [37,42,43] and references therein. We shall focus on the difference in charged magnetized plasma. On general ground, charged magnetized plasma consisting of spin one-half matter is also spin polarized with

²In fact, the magnetic susceptibility vanishes because the thermodynamic potential is linear in the magnetic field in the LLL approximation. The vanishing of susceptibility is due to cancellation between spin and orbital angular momentum contributions.

nonvanishing magnetization. It is known that medium with magnetization is gyrotropic [44], which is characterized by a polarization tensor with purely imaginary off-diagonal components. It leads to splitting of right- and left-handed electromagnetic waves. We shall see this is also true with the paramagnet. We will first present photon self-energy in charged magnetized plasma, which is then used to determine the dispersion of electromagnetic waves. We will also calculate the resummed photon propagator to be used in Sec. III.

A. Photon self-energy in charged magnetized plasma

We will use the real time formalism of finite temperature field theory in the ra basis [45]. The fields in the ra basis are related to the counterpart on the Schwinger-Keldysh contour by

$$A_r = \frac{1}{2}(A_1 + A_2), \quad A_a = A_1 - A_2. \quad (1)$$

The correlators in the ra basis are defined as

$$\begin{aligned} D_{ra}^{\mu\nu}(x) &= \langle A_r^\mu(x) A_a^\nu(0) \rangle, \\ D_{ar}^{\mu\nu}(x) &= \langle A_a^\mu(x) A_r^\nu(0) \rangle, \\ D_{rr}^{\mu\nu}(x) &= \langle A_r^\mu(x) A_r^\nu(0) \rangle, \\ D_{aa}^{\mu\nu}(x) &= \langle A_a^\mu(x) A_a^\nu(0) \rangle. \end{aligned} \quad (2)$$

The correlators in the Schwinger-Keldysh basis are given by

$$\begin{aligned} D_{11}^{\mu\nu}(x) &= \theta(x^0) \langle A^\mu(x) A^\nu(0) \rangle + \theta(-x^0) \langle A^\nu(0) A^\mu(x) \rangle, \\ D_{22}^{\mu\nu}(x) &= \theta(-x^0) \langle A^\mu(x) A^\nu(0) \rangle + \theta(x^0) \langle A^\nu(0) A^\mu(x) \rangle, \\ D_{21}^{\mu\nu}(x) &= \langle A^\mu(x) A^\nu(0) \rangle, \\ D_{12}^{\mu\nu}(x) &= \langle A^\nu(0) A^\mu(x) \rangle, \end{aligned} \quad (3)$$

corresponding to time-ordered, anti-time-ordered, greater, and lesser correlators, respectively. From (1), we can relate correlators in the two basis as

$$\begin{aligned} D_{ra}^{\mu\nu}(x) &= \frac{1}{2}(D_{11}^{\mu\nu}(x) - D_{22}^{\mu\nu}(x) - D_{12}^{\mu\nu}(x) + D_{21}^{\mu\nu}(x)), \\ D_{ar}^{\mu\nu}(x) &= \frac{1}{2}(D_{11}^{\mu\nu}(x) - D_{22}^{\mu\nu}(x) + D_{12}^{\mu\nu}(x) - D_{21}^{\mu\nu}(x)), \\ D_{rr}^{\mu\nu}(x) &= \frac{1}{4}(D_{11}^{\mu\nu}(x) + D_{22}^{\mu\nu}(x) + D_{12}^{\mu\nu}(x) + D_{21}^{\mu\nu}(x)), \\ D_{aa}^{\mu\nu}(x) &= D_{11}^{\mu\nu}(x) + D_{22}^{\mu\nu}(x) - D_{12}^{\mu\nu}(x) - D_{21}^{\mu\nu}(x). \end{aligned} \quad (4)$$

Using the explicit representations in (3) and $\theta(x^0) + \theta(-x^0) = 1$, we easily find

$$\begin{aligned}
D_{ra}^{\mu\nu}(x) &= \theta(x^0)\langle[A^\mu(x), A^\nu(0)]\rangle \equiv -iD_R^{\mu\nu}(x), \\
D_{ar}^{\mu\nu}(x) &= \theta(-x^0)\langle[A^\mu(x), A^\nu(0)]\rangle \equiv -iD_A^{\mu\nu}(x), \\
D_{rr}^{\mu\nu}(x) &= \frac{1}{2}\{A^\mu(x), A^\nu(0)\}, \\
D_{aa}^{\mu\nu}(x) &= 0,
\end{aligned} \tag{5}$$

with $D_R^{\mu\nu}(x)$ and $D_A^{\mu\nu}(x)$ being retarded and advanced correlators, respectively.

In the Schwinger-Keldysh basis, the vertices can be obtained from the interaction terms in the Lagrangian $J_1^\mu(x)A_{1,\mu}(x) - J_2^\mu(x)A_{2,\mu}(x)$. We can convert the current density $J_{1/2}$ to $J_{r/a}$ with a definition parallel to (1) to arrive at the interaction terms $J_a^\mu(x)A_{r,\mu}(x) + J_r^\mu(x)A_{a,\mu}(x)$. The photon self-energy in the ra basis is simply the correlators of current density defined as follows:

$$\begin{aligned}
\Pi_{ar}^{\mu\nu}(x) &= \langle J_r^\mu(x)J_a^\nu(0)\rangle, \\
\Pi_{ra}^{\mu\nu}(x) &= \langle J_a^\mu(x)J_r^\nu(0)\rangle, \\
\Pi_{aa}^{\mu\nu}(x) &= \langle J_r^\mu(x)J_r^\nu(0)\rangle.
\end{aligned} \tag{6}$$

Note that we use the ra labeling from the A fields for Π as is done conventionally. In particular, Π_{rr} instead of Π_{aa} vanishes identically.

Now we focus on photon self-energy in charged magnetized plasma. The retarded self-energy is defined similar to (5) with $A \rightarrow J$. The results for neutral magnetized plasma in LLL approximation have been calculated using both field theory [46] and chiral kinetic theory [47]. The inclusion of the antisymmetric part in charged magnetized plasma has also been made using field theory [30] and chiral kinetic theory [48,49], with the results in momentum space quoted below,

$$\begin{aligned}
\Pi_R^{\alpha\beta} &= -\frac{e^3 B q_3^2 u^\alpha u^\beta + q_0^2 b^\alpha b^\beta + q_0 q_3 u^{\{\alpha} b^{\beta\}}}{2\pi^2 (q_0 + i\epsilon)^2 - q_3^2} \\
&+ \frac{ie^2 \mu}{2\pi^2} \left(q_0 \epsilon^{\alpha\beta\rho\sigma} + u^{[\alpha} \epsilon^{\beta]\lambda\rho\sigma} q_\lambda^T \right) u_\rho b_\sigma,
\end{aligned} \tag{7}$$

where we have defined $A^{\{\alpha B^\beta\}} = A^\alpha B^\beta + A^\beta B^\alpha$ and $A^{[\alpha B^\beta]} = A^\alpha B^\beta - A^\beta B^\alpha$. In (7), B is the magnetic field and μ is the chemical potential for the fermion number. For simplicity, we consider medium consisting of a single species of fermion carrying positive electric charge. u^μ is fluid velocity and b^μ is the direction of the magnetic field. $q_T^\mu = b^\mu(q \cdot b) + q^\mu - u^\mu(q \cdot u)$ corresponds to spatial components of q perpendicular to b^μ . The first term of (7) is symmetric in indices with the pole coming from the chiral magnetic wave [50] in the LLL approximation. The second term is antisymmetric and purely imaginary. It comes from the Hall effect arising from the current along the drift velocity in charged plasma [48,49]. This can be confirmed in field theory [30] and in magnetohydrodynamics [51].

If we work in the local rest frame of the plasma, and point the magnetic field in the z direction so that $b^\mu = (0, 0, 0, 1)$ when $u^\mu = (1, 0, 0, 0)$, both [30,51] give $\Pi_R^{xy} = \frac{in_e}{B} q_0$ for $q_T = 0$. In the LLL approximation, we can express the electric charge density n_e in terms of electric chemical potential $\mu_e = e\mu$ and susceptibility $\chi = \frac{eB}{2\pi^2}$ as $n_e = \mu_e \chi = e\mu \frac{eB}{2\pi^2}$, which agrees with (7). The origin of the antisymmetric component implies that (7) is valid on a timescale longer than the relaxation time τ_R such that the Hall current can establish. This imposes an ultraviolet (UV) cutoff on q_0 with $q_0 \lesssim 1/\tau_R$. Beyond the cutoff, the Hall current has no time to develop, leading to no antisymmetric part in the self-energy.

B. Electromagnetic wave in magnetized plasma

We proceed to find the polarization modes for the photon by solving the Maxwell equations in the magnetized plasma. We start with the Maxwell equations in coordinate space,

$$(\partial^2 \eta^{\mu\nu} - \partial^\mu \partial^\nu) A_{\nu,r} = j_r^\mu = -i \int d^4 y \Pi_{ar}^{\mu\nu}(x, y) A_{\nu,r}. \tag{8}$$

Using (5) with $A \rightarrow J$, we can determine the following correlator in the ra basis:

$$\Pi_{ar}^{\mu\nu}(x) = -i \Pi_R^{\mu\nu}(x). \tag{9}$$

Working in momentum space and taking the Coulomb gauge $\nabla \cdot \vec{A} = 0$ in the local rest frame of the plasma, we can express the Maxwell equation as

$$Q^2 A^\mu - q_0 A_0 Q^\mu - \Pi_R^{\mu\nu} A_\nu = 0. \tag{10}$$

The polarization modes for the photon can be obtained from the solutions of q_0^2 . For pedagogical purposes, we first solve (10) for neutral plasma $\mu = 0$, in which we obtain

$$\begin{aligned}
q_0^2 &= \tilde{B} + q^2 + O(B^{-1}), & A_i &= -\frac{A_0 q_T^i q_0}{\tilde{B}}, & A_3 &= \frac{A_0 q_T^2 q_0}{\tilde{B}}, \\
q_0^2 &= q^2, & A_0 &= A_3 = 0, & q_T^i A_i &= 0,
\end{aligned} \tag{11}$$

with $\tilde{B} = e^3 B / 2\pi^2$ and $i = 1, 2$ labeling directions perpendicular to b . The first one is a gapped mode and the second one is lightlike.³

Turning to the charged plasma, we can get three roots of q_0^2 , corresponding to three polarization modes of the photon as follows:

³In the special case when $q_T = 0$, the first mode disappears and the second mode becomes two degenerate ones, as the photon does not feel the magnetic field. We are not interested in this trivial case.

$$\begin{aligned}
q_0^2 &= \tilde{B} + q^2, \\
q_0^2 &= \frac{1}{2} \left(\tilde{\mu}^2 + q_\perp^2 + 2q_3^2 - \sqrt{4\tilde{\mu}^2 q_3^2 + (q_\perp^2 + \tilde{\mu}^2)^2} \right) \equiv x_1^2, \\
q_0^2 &= \frac{1}{2} \left(\tilde{\mu}^2 + q_\perp^2 + 2q_3^2 + \sqrt{4\tilde{\mu}^2 q_3^2 + (q_\perp^2 + \tilde{\mu}^2)^2} \right) \equiv x_2^2, \quad (12)
\end{aligned}$$

with $\tilde{\mu} = e^2 \mu / 2\pi^2$ and $q_\perp^2 = q_1^2 + q_2^2$. The first mode is the same gapped one as the neutral case. The second and third correspond to the space- and timelike low energy modes, respectively. The origin of the low energy modes is most clearly seen in the neutral limit where the two modes reduce to $q_0^2 = q_3^2$ and $q_0^2 = q^2$, respectively. The former corresponds to Landau damping, which arises from energy exchange between the photon and LLL states. In the massless limit we consider, Landau damping appears as a pole instead of a cut [52]. The latter corresponds to photon dispersion in vacuum. The effect of finite density medium is to shift the two poles. The actual propagating modes are only the first and third ones in (12). One may expect to have three propagating modes rather than two due to collective motion in plasma [53]. Note that the self-energy (7) contains no explicit temperature dependence, suggesting the medium is more like a Fermi sea rather than a plasma. It follows that the number of propagating modes matches that of the vacuum. We shall elaborate on this later.

Let us take a close look at the low energy modes in the phenomenologically motivated limit

$$\tilde{\mu} \gg q: x_1^2 \approx \frac{q_3^2 q^2}{\tilde{\mu}^2}, \quad x_2^2 \approx \tilde{\mu}^2. \quad (13)$$

Now we argue that the mode x_2 actually lies outside the applicable region of (7) by making an estimate of τ_R . Note that τ_R is governed by dynamics perpendicular to the magnetic field, which is realized through the $2 \rightarrow 2$ process [29]]. We can estimate τ_R as $\tau_R^{-1} \sim e^4 \mu F((eB)^{1/2}/\mu, T/\mu)$ for some dimensionless function F . Regarding $\mu \sim T$, we easily find $x_2 \gg 1/\tau_R$. Meanwhile, the condition $x_1 \lesssim 1/\tau_R$ for mode x_1 leads to $q \lesssim (\tilde{\mu}/\tau_R)^{1/2} \sim e\tilde{\mu} \ll \tilde{\mu}$, which is consistent with our assumption in (13). To gain further insights, we plug (12) into (10) to solve for A^μ . In the same limit $\tilde{\mu} \gg q$, we obtain

$$\begin{aligned}
q_0^2 = x_1^2: \quad \frac{A_1}{A_0} &= \frac{i(q_2 q + i q_1 |q_3|)}{q_\perp^2 q} \tilde{\mu}, \\
\frac{A_2}{A_0} &= -\frac{i(q_1 q - i q_2 |q_3|)}{q_\perp^2 q} \tilde{\mu}, \quad \frac{A_3}{A_0} = \frac{q_3}{|q_3| q} \tilde{\mu}. \quad (14)
\end{aligned}$$

The physical interpretation of this mode is most transparent if we focus on the regime $q_3 \gg q_\perp$, that is a photon propagating almost along the magnetic field. We have then $\frac{A_1}{A_2} \simeq -i$ from (14). This is analogous to one of the circular polarizations in vacuum, but with the dispersion modified by the charged medium. This parity breaking mode will

play an important role in polarizing probe fermions just as a paramagnet polarizes an ordinary metal.

C. Resummed photon propagator

In the previous section, we have obtained the photon polarization modes by solving the Maxwell equations. These modes contain pole and Landau damping (also a pole in massless limit) contributions to the spectral function of the photon. In this section, we will derive the resummed photon propagator and extract the spectral function, from which we will find both pole and Landau damping contributions.

We start with the following bare photon propagators $D_{\mu\nu(0)}^{ar}$, $D_{\mu\nu(0)}^{ra}$, and $D_{\mu\nu(0)}^{rr}$ in the Coulomb gauge in thermal equilibrium,

$$\begin{aligned}
D_{\mu\nu(0)}^{ar}(Q) &= \frac{i}{(q_0 - i\epsilon)^2 - q^2} \left(P_{\mu\nu}^T + \frac{Q^2 u_\mu u_\nu}{q^2} \right), \\
D_{\mu\nu(0)}^{ra}(Q) &= \frac{i}{(q_0 + i\epsilon)^2 - q^2} \left(P_{\mu\nu}^T + \frac{Q^2 u_\mu u_\nu}{q^2} \right), \\
D_{\mu\nu(0)}^{rr}(Q) &= 2\pi \text{sgn}(q_0) \delta(Q^2) \left(\frac{1}{2} + f_\gamma(q_0) \right) \\
&\quad \times \left(P_{\mu\nu}^T + \frac{Q^2}{q^2} u_\mu u_\nu \right), \quad (15)
\end{aligned}$$

with $\text{sgn}(q_0)$ being the sign function and $f_\gamma(q_0)$ being the Bose-Einstein distribution function $f_\gamma(q_0) = 1/(\exp(q_0/T) - 1)$. The structures $P_{\mu\nu}^T$ and $\frac{Q^2}{q^2} u_\mu u_\nu$ correspond to transverse and longitudinal components of the propagator, respectively. The transverse projection operator $P_{\mu\nu}^T$ is defined as $P_{\mu\nu}^T = P_{\mu\nu} - \frac{P_{\mu\alpha} P_{\nu\beta} Q^\alpha Q^\beta}{-Q^2 + (Q \cdot u)^2}$ with $P_{\mu\nu} = u_\mu u_\nu - \eta_{\mu\nu}$ being the projection operator orthogonal to fluid velocity. In the fluid's rest frame, we have

$$\begin{aligned}
P_{00}^T &= P_{0i}^T = P_{i0}^T = 0, \\
P_{ij}^T &= \delta_{ij} - \frac{q_i q_j}{q^2}. \quad (16)
\end{aligned}$$

Using the definitions (2) and (6) and the couplings $J_a^\mu(x) A_{r,\mu}(x) + J_r^\mu(x) A_{a,\mu}(x)$, we may express the propagators up to first order in the self-energy as

$$\begin{aligned}
\left(\begin{array}{cc} D^{rr} & D^{ra} \\ D^{ar} & 0 \end{array} \right)_{\mu\nu} &= \left(\begin{array}{cc} D_{(0)}^{rr} & D_{(0)}^{ra} \\ D_{(0)}^{ar} & 0 \end{array} \right)_{\mu\nu} - \left(\begin{array}{cc} D_{(0)}^{rr} & D_{(0)}^{ra} \\ D_{(0)}^{ar} & 0 \end{array} \right)_{\mu\alpha} \\
&\quad \times \left(\begin{array}{cc} 0 & \Pi^{ra} \\ \Pi^{ar} & \Pi^{aa} \end{array} \right)^{\alpha\beta} \left(\begin{array}{cc} D_{(0)}^{rr} & D_{(0)}^{ra} \\ D_{(0)}^{ar} & 0 \end{array} \right)_{\beta\nu}. \quad (17)
\end{aligned}$$

By iteration, we deduce that the resummed propagators satisfy the following equations:

$$\begin{aligned} \begin{pmatrix} D^{rr} & D^{ra} \\ D^{ar} & 0 \end{pmatrix}_{\mu\nu} &= \begin{pmatrix} D^{rr}_{(0)} & D^{ra}_{(0)} \\ D^{ar}_{(0)} & 0 \end{pmatrix}_{\mu\nu} - \begin{pmatrix} D^{rr}_{(0)} & D^{ra}_{(0)} \\ D^{ar}_{(0)} & 0 \end{pmatrix}_{\mu\alpha} \\ &\times \begin{pmatrix} 0 & \Pi^{ra} \\ \Pi^{ar} & \Pi^{aa} \end{pmatrix}^{\alpha\beta} \begin{pmatrix} D^{rr} & D^{ra} \\ D^{ar} & 0 \end{pmatrix}_{\beta\nu}. \end{aligned} \quad (18)$$

The component form of the above reads

$$\begin{aligned} D^{ra}_{\mu\nu} &= D^{ra}_{\mu\nu(0)} - D^{ra}_{\mu\alpha(0)} \Pi^{ab}_{ar} D^{ra}_{\beta\nu}, \\ D^{ar}_{\mu\nu} &= D^{ar}_{\mu\nu(0)} - D^{ar}_{\mu\alpha(0)} \Pi^{ab}_{ra} D^{ar}_{\beta\nu}, \\ D^{rr}_{\mu\nu} &= D^{rr}_{\mu\nu(0)} - D^{ra}_{\mu\alpha(0)} \Pi^{ab}_{ar} D^{rr}_{\beta\nu} \\ &\quad - \left(D^{rr}_{\mu\alpha(0)} \Pi^{ab}_{ra} + D^{ra}_{\mu\alpha(0)} \Pi^{ab}_{aa} \right) D^{ar}_{\beta\nu}. \end{aligned} \quad (19)$$

The resummed propagators can be solved by inverting the following matrix equations:

$$\begin{aligned} \left(\delta_{\alpha}^{\mu} + D^{ra}_{\alpha\beta(0)} \Pi^{\beta\mu}_{ar} \right) D^{ra}_{\mu\nu} &= D^{ra}_{\alpha\nu(0)}, \\ \left(\delta_{\alpha}^{\mu} + D^{ar}_{\alpha\beta(0)} \Pi^{\beta\mu}_{ra} \right) D^{ar}_{\mu\nu} &= D^{ar}_{\alpha\nu(0)}, \\ \left(\delta_{\alpha}^{\mu} + D^{ra}_{\alpha\rho(0)} \Pi^{\rho\mu}_{ar} \right) D^{rr}_{\mu\nu} &= \left(D^{rr}_{\alpha\nu(0)} - D^{rr}_{\alpha\beta(0)} \Pi^{\beta\sigma}_{ra} D^{ar}_{\sigma\nu} \right. \\ &\quad \left. - D^{ra}_{\alpha\beta(0)} \Pi^{\beta\sigma}_{aa} D^{ar}_{\sigma\nu} \right). \end{aligned} \quad (20)$$

We first invert the first two equations to obtain $D^{ra}_{\mu\nu}(Q)$ and $D^{ar}_{\mu\nu}(Q)$, and then use the results to invert the last equation to obtain $D^{rr}_{\mu\nu}$. Note that our knowledge about the self-energy from the LLL approximation should be viewed as leading terms in the limit $B \rightarrow \infty$. It follows that we should also keep only the leading terms in the resulting resummed propagators, which gives the following results:

$$\begin{aligned} D^{ra}_{\mu\nu}(Q) &= \left(\frac{1}{(q_0 + i\epsilon)^2 - x_1^2} + \frac{1}{(q_0 + i\epsilon)^2 - x_2^2} \right) \\ &\quad \times \frac{A_{\mu\nu}(Q)\tilde{\mu} + S_{\mu\nu}(Q)}{(q_0^2 - x_1^2) + (q_0^2 - x_2^2)}, \\ D^{ar}_{\mu\nu}(Q) &= D^{ra}_{\nu\mu}(-Q), \\ D^{rr}_{\mu\nu}(Q) &= -2i\pi\text{sgn}(q_0)(S_{\mu\nu}(Q) + A_{\mu\nu}(Q)\tilde{\mu}) \left(\frac{1}{2} + f_{\gamma}(q_0) \right) \\ &\quad \times \left(\frac{\delta(q_0^2 - x_1^2)}{q_0^2 - x_2^2} + \frac{\delta(q_0^2 - x_2^2)}{q_0^2 - x_1^2} \right). \end{aligned} \quad (21)$$

Here $A_{\mu\nu}$ and $S_{\mu\nu}$ are the antisymmetric and symmetric tensors defined, respectively, as

$$\begin{aligned} A_{\mu\nu}(Q) &= -\frac{q_0}{q^2} \left(q_0 u_{[\mu} \epsilon_{\nu\lambda\rho\sigma]} q_T^{\lambda} u^{\rho} b^{\sigma} - q_3^2 \epsilon_{\mu\nu\rho\sigma} u^{\rho} b^{\sigma} \right. \\ &\quad \left. + q_3 b_{[\mu} \epsilon_{\nu\lambda\rho\sigma]} q_T^{\lambda} u^{\rho} b^{\sigma} \right), \\ S_{\mu\nu}(Q) &= i(-g_{\mu\nu}(q_0^2 - q_3^2) - q_3^2 u_{\mu} u_{\nu} - q_0^2 b_{\mu} b_{\nu} - b_{\{\mu} u_{\nu\}} q_0 q_3) \\ &\quad + \frac{i}{q^2} (u_{\{\mu} q_{\nu\}} q_3^3 + b_{\{\mu} q_{\nu\}} q_0^2 q_3) \\ &\quad + \frac{i}{q^4} q_{\mu} q_{\nu} (q^2 q_3^2 - q_0^2 (q^2 + q_3^2)). \end{aligned} \quad (22)$$

Clearly, the low energy modes found in Sec. II B are present as poles of $D^{ra}_{\mu\nu}(Q)$ and $D^{ar}_{\mu\nu}(Q)$. The gapped mode in Sec. II B is invisible after the limit $B \rightarrow \infty$ is taken in the resummed propagator. From the definition (2), it is easy to show that $D^{rr}_{\mu\nu}(Q)$ is Hermitian. This is indeed satisfied by the corresponding expression in (21) with real symmetric and purely imaginary antisymmetric components.

III. PROBE FERMION IN A PARAMAGNET

We consider a probe fermion interacting with the medium. We choose an unmagnetized probe fermion. This is motivated by heavy ion phenomenology: with the quick decay of the magnetic field, the strange quarks produced at later stage are not spin polarized and can only interact with the medium. We shall consider the high density limit $\tilde{\mu} \gg q$. In this case the medium is like a paramagnet, which is able to polarize the probe fermion. We will corroborate the picture with calculations of damping rates of probe fermions. For simplicity, we take the probe fermion to be massless.

A. Resummed fermion propagator and damping rate

A probe fermion interacting with the medium will have a modified dispersion, with the damping rate given by the imaginary part of the pole in the resummed retarded propagator. The procedure of deriving the resummed propagator is similar to that in Sec. II C. We start with the bare fermion propagators in the ra basis,

$$\begin{aligned} S_{ar(0)}(P) &= \frac{i\not{P}}{(p_0 - i\epsilon)^2 - p^2}, \\ S_{ra(0)}(P) &= \frac{i\not{P}}{(p_0 + i\epsilon)^2 - p^2}, \\ S_{rr(0)}(P) &= \left(\frac{1}{2} - f_e(p_0) \right) 2\pi\text{sgn}(p_0)\not{P}\delta(P^2), \end{aligned} \quad (23)$$

with f_e being the Fermi-Dirac distribution function $f_e(p_0) = 1/(\exp(p_0/T) + 1)$. For the probe fermion, we set $f_e = 0$. The resummation equation for the retarded propagator is analogous to its counterpart in (20),

$$S_{ra}(P) = S_{ra(0)}(P) - S_{ra(0)}(P)\Sigma_{ar}(P)S_{ra}(P). \quad (24)$$

The self-energy in (24) is defined by the Fourier transform of the following:

$$\Sigma_{ar}(x) = \langle \eta_r \bar{\eta}_a \rangle, \quad (25)$$

$$S_{ra} = \frac{i}{\not{P} + i\Sigma_{ar}}, \quad (26)$$

where we have dropped the $i\epsilon$ assuming the self-energy Σ_{ar} already shifts the pole of p_0 from the real axis. Since both the medium and probe fermions are chiral, the self-energy also preserves the chiral symmetry with the following decomposition:

$$\Sigma_{ar} = \mathcal{V}_\mu \gamma^\mu + \mathcal{A}_\mu \gamma^5 \gamma^\mu, \quad (27)$$

with \mathcal{A}_μ and \mathcal{V}_μ being the vector and axial vector, respectively. The decoupling of left- and right-handed components is manifest in the chiral representation of Dirac matrices, with the following explicit denominator of (26):

$$\not{P} + i\Sigma_{ar} = \begin{pmatrix} (P_\mu + i\mathcal{V}_\mu - i\mathcal{A}_\mu)\sigma^\mu & \\ & (P_\mu + i\mathcal{V}_\mu + i\mathcal{A}_\mu)\bar{\sigma}^\mu \end{pmatrix}. \quad (28)$$

This allows us to treat left- and right-handed components separately as

$$S_{ra}^R = \frac{i}{(P_\mu + i\mathcal{V}_\mu - i\mathcal{A}_\mu)\sigma^\mu} = \frac{i(P_\mu + i\mathcal{V}_\mu - i\mathcal{A}_\mu)\bar{\sigma}^\mu}{(P + i\mathcal{V} - i\mathcal{A})^2},$$

$$S_{ra}^L = \frac{i}{(P_\mu + i\mathcal{V}_\mu + i\mathcal{A}_\mu)\bar{\sigma}^\mu} = \frac{i(P_\mu + i\mathcal{V}_\mu + i\mathcal{A}_\mu)\sigma^\mu}{(P + i\mathcal{V} + i\mathcal{A})^2}. \quad (29)$$

It is clear that the effect of self-energy is to shift the momenta of left- and right-handed components respectively. The coefficient \mathcal{A} encodes the splitting between left- and right-handed components. At finite charge density, the medium is spin polarized. We suggest in Sec. II B that the Landau damping mode is parity breaking. Thus, we expect splitting between left- and right-handed components.

Now we present explicit calculation of the self-energy. Figure 1 shows one of the self-energy diagrams in the ra basis. The other diagram with ra labelings of fermion and photon exchanged does not give rise to damping because the temperature factor expected in the damping rate cannot enter with the fermion being not thermally populated. The corresponding self-energy contribution is given by⁴

$$\Sigma_{ar}(P) = e^2 \int \frac{d^4 Q}{(2\pi)^4} \gamma^\mu S_{ra(0)}(P-Q) \gamma^\nu D_{\mu\nu}^{rr}(Q). \quad (30)$$

⁴With our definition (25), the interaction vertex is $-e$ instead of $-ie$. The factor $i^2 = -1$ appears in the resummation equation (24).

B. Damping in a paramagnet

Now we evaluate the self-energy in the high density limit $\tilde{\mu} \gg q$. We have shown in Sec. II B that only the Landau damping mode survives in this limit. We then evaluate the integrals with (23) and (21) taking contribution from $q_0^2 = x_1^2$ only. We calculate separately antisymmetric and symmetric contributions to be denoted as Σ_{ar}^A and Σ_{ar}^S . The antisymmetric contribution reads

$$\Sigma_{ar}^A(P) = \frac{e^2}{(2\pi)^3} \int \frac{d^4 Q \text{sgn}(q_0)}{(P-Q)^2 + i\epsilon(p_0 - q_0)} \left(\frac{1}{2} + f_\gamma(q_0) \right) \times \left(\frac{\delta(q_0^2 - x_1^2)}{q_0^2 - x_2^2} + \frac{\delta(q_0^2 - x_2^2)}{q_0^2 - x_1^2} \right) \times \gamma^\mu (\not{P} - \not{Q}) \gamma^\nu A_{\mu\nu}(Q) \tilde{\mu}. \quad (31)$$

We first deal with $\gamma^\mu (\not{P} - \not{Q}) \gamma^\nu A_{\mu\nu}(Q)$ by using the following relation:

$$\gamma^\mu \gamma^\alpha \gamma^\nu = g^{\mu\alpha} \gamma^\nu - g^{\mu\nu} \gamma^\alpha + g^{\alpha\nu} \gamma^\mu - i\epsilon^{\mu\alpha\nu\beta} \gamma^5 \gamma_\beta. \quad (32)$$

Only the last antisymmetric term contributes when contracted with $A_{\mu\nu}$, giving

$$\gamma^\mu (\not{P} - \not{Q}) \gamma^\nu A_{\mu\nu}(Q) = -i(P-Q)_\alpha \epsilon^{\mu\alpha\nu\beta} \gamma^5 \gamma_\beta A_{\mu\nu}(Q) = \frac{2i}{q^2} (q_0^2 f_1 + q_0 f_2) \quad (33)$$

with

$$f_1 = (\mathbf{p}_\perp \cdot \mathbf{q}_\perp - q^2) \gamma^5 \gamma^3 - p_3 \gamma^5 \mathbf{q}_\perp \cdot \boldsymbol{\gamma}_\perp,$$

$$f_2 = p_0 q_3^2 \gamma^5 \gamma^3 + p_0 q_3 \gamma^5 \mathbf{q}_\perp \cdot \boldsymbol{\gamma}_\perp + q_3 \gamma^5 \gamma^0 (q^2 - \mathbf{p} \cdot \mathbf{q}), \quad (34)$$

being the coefficients of even and odd powers of q_0 . The perpendicular vectors are defined as $\mathbf{p}_\perp = (p_1, p_2)$ and similarly for \mathbf{q}_\perp and $\boldsymbol{\gamma}_\perp$.

We proceed by making several approximations: First, the self-energy induces only a small correction to the dispersion, so for the purpose of finding the damping rate of an on-shell probe fermion we may set $P^2 = 0$. Second, the Landau damping mode is nearly static, allowing us to approximate $\frac{1}{2} + f_\gamma(Q) \simeq \frac{T}{q_0}$. Third, combining the on-shell condition and $q_0 \ll q \ll p_0$, we approximate the denominator of fermion propagator as

$$\frac{1}{(P-Q)^2 + i\epsilon(p_0 - q_0)} \simeq \frac{1}{2} \frac{1}{(\mathbf{p} \cdot \mathbf{q} + i\epsilon p_0)}, \quad (35)$$

dropping $Q^2 \ll 2P \cdot Q$ and $q_0 p_0$. Then, (31) can be written as

$$\begin{aligned} \Sigma_{ar}^A(P) &= -\frac{ie^2T}{(2\pi)^3\tilde{\mu}} \int \frac{d^3q}{q^2(\mathbf{p}\cdot\mathbf{q} + i\epsilon p_0)} \\ &\quad \times \int \frac{dq_0}{q_0} \delta\left(q_0^2 - \frac{q_3^2 q^2}{\tilde{\mu}^2}\right) \text{sgn}(q_0)(q_0^2 f_1 + q_0 f_2). \end{aligned} \quad (36)$$

We proceed with the integral of q_0 first. Since f_1 and f_2 are independent of q_0 , the integral receives contribution from the integrand even in q_0 as

$$\begin{aligned} &\int \frac{dq_0}{q_0} \delta\left(q_0^2 - \frac{q_3^2 q^2}{\tilde{\mu}^2}\right) \epsilon(q_0)(q_0^2 f_1 + q_0 f_2) \\ &= f_1 \int dq_0 \delta\left(q_0^2 - \frac{q_3^2 q^2}{\tilde{\mu}^2}\right) q_0 \text{sgn}(q_0) = f_1. \end{aligned} \quad (37)$$

The remaining integrals are evaluated using the residue theorem. The details can be found in the Appendix. We quote the final results here. To be specific, we take $p_0 > 0$ to arrive at the following results:

$$\Sigma_{ar}^A(P) = -ic_1\gamma^5\gamma^3 + ic_2\gamma^5\mathbf{p}_\perp \cdot \boldsymbol{\gamma}_\perp + c_3\gamma^5\gamma^3, \quad (38)$$

with

$$\begin{aligned} c_1 &= \frac{e^2Tq_{UV}}{4\pi\tilde{\mu}} \left(1 - \frac{|p_3|}{p}\right), \quad c_2 = \frac{e^2Tq_{UV}}{4\pi\tilde{\mu}} \left(1 - \frac{|p_3|}{p}\right) \frac{p_3}{p_\perp^2}, \\ c_3 &= \frac{e^2Tq_{UV}^2}{8\pi\tilde{\mu}|p_3|}, \end{aligned} \quad (39)$$

where q_{UV} is the UV cutoff for q , which can be taken as $q_{UV} \sim e\tilde{\mu}$ based on the discussion below (13).

The calculation of the symmetric contribution proceeds similarly. We simply quote the final result, collecting details in the Appendix. For $p_0 > 0$, we have

$$\Sigma_{ar}^S = \gamma^0 d_1 + i\mathbf{p}_\perp \cdot \boldsymbol{\gamma}_\perp d_2 + i\gamma^3 d_3, \quad (40)$$

with

$$\begin{aligned} d_1 &= \frac{e^2T p_0 \ln \frac{q_{UV}}{q_{IR}}}{4\pi p}, \quad d_2 = \frac{e^2T q_{UV}}{4\pi p_\perp^2} \left(1 - \frac{|p_3|}{p}\right), \\ d_3 &= \frac{e^2T q_{UV}}{4\pi p} \text{sgn}(p_3), \end{aligned} \quad (41)$$

where q_{IR} is the infrared (IR) cutoff of q_\perp . We will discuss the meaning of the IR cutoff shortly.

Now we can take $\Sigma_{ar} = \Sigma_{ar}^A + \Sigma_{ar}^S$ and compare with (27) and (29) to obtain damping rates of left- and right-handed components, respectively. We find it more instructive to obtain the contributions to the damping rate from Σ_{ar}^A and Σ_{ar}^S , respectively. In fact, if we keep linear order in Σ_{ar}^A and Σ_{ar}^S , the corresponding shifts of the poles from the

vacuum counterpart are additive. The imaginary part of the shift gives the damping rate. We first consider contribution from Σ_{ar}^A . Using (27) and (29), we easily find the poles given by

$$\begin{aligned} L: p_0 &\simeq p + \frac{c_2 p_\perp^2}{p} - \frac{c_1 p_3}{p} - \frac{ic_3 p_3}{p} = p - \frac{ic_3 p_3}{p}, \\ R: p_0 &\simeq p - \frac{c_2 p_\perp^2}{p} + \frac{c_1 p_3}{p} + \frac{ic_3 p_3}{p} = p + \frac{ic_3 p_3}{p}. \end{aligned} \quad (42)$$

We can see Σ_{ar}^A causes the shifts of poles with opposite sign for both real and imaginary parts. The real part would lead to the chiral shift discussed in [54], but vanishes when explicit expressions for c_1 and c_2 are used. The imaginary part gives the following damping rates:

$$\begin{aligned} \Gamma_L &\simeq \frac{c_3 p_3}{p} = \frac{e^2 T q_{UV}^2}{8\pi\tilde{\mu}p} \text{sgn}(p_3), \\ \Gamma_R &\simeq -\frac{c_3 p_3}{p} = -\frac{e^2 T q_{UV}^2}{8\pi\tilde{\mu}p} \text{sgn}(p_3). \end{aligned} \quad (43)$$

The cases with $\Gamma < 0$ are unstable. These include right-handed components with $p_3 > 0$ and left-handed components with $p_3 < 0$. The implication is interesting: Because of spin-momentum locking, both cases have a positive spin component along the direction of the paramagnet. Interaction with the paramagnet tends to polarize the probe fermion by amplifying these modes. In contrast, left-handed components with $p_3 > 0$ and right-handed components with $p_3 < 0$ have $\Gamma > 0$. They both have a negative spin component along the direction of the paramagnet and are damped out. This provides a mechanism to polarize the probe fermion.

Now we turn to the symmetric contribution. This contribution leads to identical shifts for the left- and right-handed components,

$$p_0 \simeq p + \frac{p_\perp^2 d_2}{p} + \frac{p_3 d_3}{p} - id_1 = p + \frac{e^2 T q_{UV}}{4\pi p} - id_1. \quad (44)$$

The corresponding damping rate is given by

$$\Gamma = d_1 = \frac{e^2 T p_0 \ln \frac{q_{UV}}{q_{IR}}}{4\pi p}. \quad (45)$$

It depends on both UV and IR cutoffs. While the UV cutoff is set by $q_{UV} \sim e\tilde{\mu}$, the IR cutoff is fictitious. The appearance of the logarithmic divergence is not new. By using the resummed photon propagator, we have softened the $\int dq/q^3$ IR divergence typical in Coulomb scattering into a logarithmic one. The persistence of logarithmic divergence indicates the corresponding damping is

nonexponential in time, which can be obtained with more sophisticated resummation [55]. Since we are mainly concerned with the splitting in damping rates, we shall not attempt further resummation as in [55].

Combining the contributions from antisymmetric and symmetric parts, we obtain a slightly modified picture: a probe fermion interacting with the medium will generically be damped. This is because the damping rate from the symmetric contribution is parametrically larger than the counterpart from the antisymmetric contribution: $d_1 \sim e^2 T \gg \frac{c_3 |p_3|}{p} \sim \frac{e^6 T \mu}{p}$ using $q_{UV} \sim e \tilde{\mu}$. However, with the medium being like a paramagnet, modes with a positive/negative spin component along the direction of the paramagnet have smaller/larger damping rate, thus interaction tends to polarize the probe fermion. This occurs at a timescale $t \sim \Delta \Gamma^{-1} \sim \frac{p}{e^6 T \mu}$. One may worry that, at this timescale, the probe fermion has been damped out completely because of the hierarchy $d_1 \gg \frac{c_3 |p_3|}{p}$. This can still have physical consequence. If the probe fermion is continuously produced in the medium, the number density can be maintained despite damping by the medium, but the polarization mechanism from the splitting of damping rates always works. We will extend the analysis to QGP case in the next section, where we will see the splitting of damping rates can be parametrically enhanced, making the polarization dynamics more efficient.

IV. PROBE QUARK IN A PARAMAGNET OF QGP

Now we extend the analysis to a probe quark in charged QGP. A new feature in this case is that gluon self-energy receives an additional contribution from gluon self-interaction. It follows that the dispersions we obtain from solving Maxwell equations no longer apply. We will identify low energy modes by finding the resummed gluon propagator and use it to calculate the splitting of damping rates for the probe quark.

A. Gluon propagator in charged QGP

We follow the procedure in Sec. II C. The gluon bare propagator in the Coulomb gauge is the same as (15) except for additional color structures,

$$\begin{aligned} D_{\mu\nu(0)}^{AB,ar} &= \delta^{AB} D_{\mu\nu(0)}^{ar}, \\ D_{\mu\nu(0)}^{AB,ra} &= \delta^{AB} D_{\mu\nu(0)}^{ra}, \\ D_{\mu\nu(0)}^{AB,rr} &= \delta^{AB} D_{\mu\nu(0)}^{rr}. \end{aligned} \quad (46)$$

We have used capital letters for color indices and the color structure is diagonal δ^{AB} . The gluon self-energy is given by

$$\begin{aligned} \Pi_R^{\mu\nu,AB} &= \left[\frac{g^2 e B q_3^2 u^\mu u^\nu + q_0^2 b^\mu b^\nu + q_0 q_3 u^{[\mu} b^{\nu]}}{2\pi^2 (q_0 + i\epsilon)^2 - q_3^2} \right. \\ &\quad + \frac{i g^2 \mu}{2\pi^2} \frac{1}{2} \left(q_0 \epsilon^{\mu\nu\rho\sigma} + u^{[\mu} \epsilon^{\nu]\lambda\rho\sigma} q_\lambda^T \right) u_\rho b_\sigma \\ &\quad \left. - P_T^{\mu\nu} \Pi_T - P_L^{\mu\nu} \Pi_L \right] \delta^{AB}, \end{aligned} \quad (47)$$

with $\Pi_{T/L}$ being the transverse/longitudinal components from the gluon loop. The explicit expressions in the hard thermal loop (HTL) regime are as follows:

$$\begin{aligned} \Pi_T &= m^2(x^2 + (1-x^2)xQ_0(x)), \\ \Pi_L &= -2m^2(x^2 - 1)(1 - xQ_0(x)), \end{aligned} \quad (48)$$

where $m^2 = \frac{1}{6} N_c g^2 T^2$ is the thermal mass and N_c is the number of colors. The Legendre function Q_0 is defined as $Q_0(x) = \frac{1}{2} \ln \left| \frac{x+1}{x-1} \right| - \frac{i\pi}{2} \theta(1-x^2)$. The symmetric components of (47) have been extensively discussed in [56]. The antisymmetric component is obtained by a straightforward generalization of the calculations in [30] for a single species of quark carrying positive electric charge $q_f > 0$, with μ being the chemical potential for quark number density. The overall factor $\frac{1}{2}$ comes from color trace in the fundamental representation $\text{tr}[t^A t^B] = \frac{1}{2} \delta^{AB}$. The physical interpretation is the chromo-Hall effect. Imagine applying a chromoelectric field in color direction A perpendicular to the magnetic field. The quarks carrying both electric charge q_f and effective chromocharge \bar{g} will develop a drift velocity $v^A = \frac{\bar{g} E^A}{q_f B}$ where the chromoelectric force and ordinary Lorentz force reaches a balance. This gives rise to a chromocurrent along the drift velocity

$$J^A = \bar{g} \rho v^A = \frac{\bar{g}^2 E^A}{q_f B} \chi \mu = \bar{g}^2 E^A \mu, \quad (49)$$

where we have used $\chi = q_f B$. To arrive at (47), we need to fix the effective chromocharge. This is most easily done in double line basis for color [57], in which the gluon color index is represented as $A = ij$ and quark color indices are represented by i and j . The color matrices in fundamental representation are given by

$$t_{kl}^{ij} = \frac{1}{\sqrt{2}} \left(\delta_k^i \delta_l^j - \frac{1}{N_c} \delta^{ij} \delta_{kl} \right). \quad (50)$$

It is most easily understood in the large N_c limit, in which the color indices of gluons and quarks are locked. Naturally, the corresponding quarks lead to chromocurrent in the same color direction as the chromoelectric field with the effective charge $\bar{g} = \frac{1}{\sqrt{2}} g$, thus the factor $\frac{1}{2}$ is perfectly accounted for.

Since the color structure is trivial in both bare propagator and self-energy, we can simply ignore it and then use (19) to obtain the resummed gluon propagator. We assume the following hierarchy: $eB \gg T^2$, $eB \gg \mu q$ and expand to leading order in B^{-1} . The resulting resummed propagator

$$D_{\mu\nu}^{ra,A}(Q) = -q^2 Q^2 \left[-q^6(q_0^2 - q_3^2) + q_0^2 q_3^2 (q_0^2 - \Pi_T)(\Pi_T - \Pi_L) + q^4 [2q_0^4 + 2q_3^2 \Pi_T - q_0^2 (2q_3^2 + \bar{\mu}^2 + \Pi_T + \Pi_L)] \right. \\ \left. + q^2 [-q_0^6 + q_3^2 \Pi_T^2 + q_0^4 (q_3^2 + \bar{\mu}^2 + \Pi_T + \Pi_L) + q_0^2 (q_3^2 (\Pi_L - 3\Pi_T) - \Pi_T \Pi_L)] \right]^{-1} A_{\mu\nu} \bar{\mu},$$

$$D_{\mu\nu}^{ar,A}(Q) = D_{\nu\mu}^{ra,A}(-Q),$$

$$D_{\mu\nu}^{rr,A}(Q) = (D_{\mu\nu}^{ra,A}(Q) - D_{\mu\nu}^{ar,A}(Q)) \left(\frac{1}{2} + f_g(q_0) \right), \quad (51)$$

with $\bar{\mu} = \frac{\tilde{q}\mu}{2\pi}$ as analog of $\tilde{\mu}$. It should be understood that $q_0 \rightarrow q_0 + i\epsilon$ is needed in the first explicit expression. The resummed rr propagator is constructed using spectral representation, with $D_{\mu\nu}^{ra,A}(Q) - D_{\mu\nu}^{ar,A}(Q)$ giving the anti-symmetric part of the spectral function and f_g being Bose-Einstein distribution for gluons. It is worth noting that (51) and (21) share the same Lorentz structure, but very different spectral function. The spectral function arises from collective excitations as well as Landau dampings. The Landau damping can give both pole and cut contributions from gluon-quark (in the LLL state) scatterings and gluon-gluon scatterings, respectively.

To simplify the analysis, we consider two limits where either one of them dominates: $\bar{\mu}^2 \gg \Pi_{T/L}$ (high density limit) and $\bar{\mu}^2 \ll \Pi_{T/L}$ (low density limit). Note that $\Pi_{T/L} \sim g^2 T^2$. The former limit requires parametrically

contains both symmetric and antisymmetric parts. The symmetric part exists in the absence of μ . It does not lead to splitting of the damping rate so we do not keep track of it. The antisymmetric part is given by (suppressing the color structure)

large μ or small T : $g^2 \mu \gg T$. In this case, we may ignore $\Pi_{T/L}$ and the rr propagator reduces to the QED counterpart (21) with the substitution $\tilde{\mu} \rightarrow \bar{\mu}$,

$$D_{\mu\nu}^{rr,A}(Q) = -2i\pi \text{sgn}(q_0) \left(\frac{1}{2} + f_g(q_0) \right) \\ \times \left(\frac{\delta(q_0^2 - \bar{x}_1^2)}{q_0^2 - \bar{x}_2^2} + \frac{\delta(q_0^2 - \bar{x}_2^2)}{q_0^2 - \bar{x}_1^2} \right) A_{\mu\nu}(Q) \bar{\mu}. \quad (52)$$

We have used $\bar{x}_{1,2}$ to denote $x_{1,2}(\tilde{\mu} \rightarrow \bar{\mu})$. Like in the QED case, the spectral function contains Landau damping poles and lightlike modes, both modified by density. The latter limit is close to the usual magnetized plasma limit, where the density leads to the following rr propagator:

$$D_{\mu\nu}^{rr,A}(Q) = 2i \text{Im} \left[\frac{Q^2 q^2}{(Q^2 - \Pi_T)(q^2 Q^2 (q_0^3 - q_3^3) - Q^2 q_3^2 \Pi_T - q_0^2 q_\perp^2 \Pi_L)} \right] \left(\frac{1}{2} + f_g(q_0) \right) A_{\mu\nu} \bar{\mu}. \quad (53)$$

The spectral function contains two poles and cut. The poles are located at

$$Q^2 - \Pi_T = 0, \\ q^2 Q^2 (q_0^3 - q_3^3) - Q^2 q_3^2 \Pi_T - q_0^2 q_\perp^2 \Pi_L = 0. \quad (54)$$

Not surprisingly they correspond to the transverse mode and mixed mode in the HTL regime in the absence of μ [56]. The location of the cut is at $Q^2 < 0$, from Landau damping. Although the antisymmetric part inherits most spectral features from the symmetric part, there is one difference: the transverse mode and mixed mode are decoupled in the symmetric part, but are coupled in the antisymmetric part in the form of product in (53).

B. Damping rate of probe quark

Now we can proceed to calculate the splitting of damping rates from antisymmetric part of the gluon propagator. Similar to (30), we have for the quark self-energy

$$\Sigma_{ar}(P) = \frac{N_c^2 - 1}{2N_c} g^2 \int \frac{d^4 Q}{(2\pi)^4} \gamma^\mu S_{ra(0)}(P-Q) \gamma^\nu D_{\mu\nu}^{rr}(Q), \quad (55)$$

where the overall factor comes from $t^A t^A = \frac{N_c^2 - 1}{2N_c}$. The integration of Q should be bounded by the applicable region of chromo-Hall dynamics, which will be fixed by $q_0 \lesssim \tau_R^{-1}$.

We first calculate the damping rate in the high density limit $\bar{\mu}^2 \gg \Pi_{T/L}$. Using (52), (55), and (23), we have

$$\begin{aligned}\Sigma_{ar}^A(P) &= \frac{N_c^2 - 1}{2N_c} \frac{g^2}{(2\pi)^3} \int \frac{d^4 Q \text{sgn}(q_0)}{(P - Q)^2 + i\epsilon(p_0 - q_0)} \\ &\times \left(\frac{1}{2} + f_g(q_0) \right) \left(\frac{\delta(q_0^2 - \bar{x}_1^2)}{q_0^2 - \bar{x}_2^2} + \frac{\delta(q_0^2 - \bar{x}_2^2)}{q_0^2 - \bar{x}_1^2} \right) \\ &\times \gamma^\mu (\not{P} - \not{Q}) \gamma^\nu A_{\mu\nu}(Q) \bar{\mu}. \quad (56)\end{aligned}$$

The γ matrices are evaluated in the same way as before,

$$\gamma^\mu (\not{P} - \not{Q}) \gamma^\nu A_{\mu\nu}(Q) = \frac{2i}{q^2} (q_0^2 f_1 + q_0 f_2), \quad (57)$$

with f_1 and f_2 taking the schematic forms $c_\mu \gamma^5 \gamma^\mu$ and c_μ being real functions of P and Q . We make the following observation: the damping rate arises from purely imaginary shift of momentum. This corresponds to the real part of the coefficients of $\gamma^5 \gamma^\mu$ in Σ_{ar}^A . It is only possible when the $i\epsilon$ prescription is invoked in the integral. It amounts to keeping the real part of the following:

$$\begin{aligned}\text{Re} \frac{i}{(P - Q)^2 + i\text{sgn}(p_0 - q_0)} \\ = \pi \delta((P - Q)^2) \text{sgn}(p_0 - q_0).\end{aligned} \quad (58)$$

Taking $P^2 = 0$ as before and $p_0 > 0$, we have the $\delta((P - Q)^2) \simeq \delta(2P \cdot Q)$. The Dirac δ function is non-vanishing for spacelike Q only, which comes from the mode $q_0^2 = \bar{x}_1^2$. This is the density modified Landau damping pole. If we further estimate the relaxation time in the high density limit $\tau_R^{-1} \sim g^4 \mu G((eB)^{1/2}/\mu)$ for some dimensionless function G . The condition $x_1 \lesssim 1/\tau_R$ leads to $q \lesssim g\bar{\mu} \ll \bar{\mu}$ similar to the QED case. Also, the mode becomes almost static as $x_1^2 \simeq \frac{q_3^2 q^2}{\bar{\mu}^2} \ll q^2$. The remaining analysis is parallel to the QED case. We can easily obtain the damping rate by the substitution $\tilde{\mu} \rightarrow \bar{\mu}$ in (43),

$$\begin{aligned}\Gamma_L &\simeq \frac{N_c^2 - 1}{2N_c} \frac{g^2 T q_{UV}^2}{8\pi \bar{\mu} p} \text{sgn}(p_3), \\ \Gamma_R &\simeq -\frac{N_c^2 - 1}{2N_c} \frac{g^2 T q_{UV}^2}{8\pi \bar{\mu} p} \text{sgn}(p_3),\end{aligned} \quad (59)$$

with $q_{UV} \sim g\bar{\mu}$. Clearly QGP in this limit behaves like a paramagnet, which amplifies/damps modes with positive/negative spin components along the magnetic field, respectively.

Now we move on to the limit $\bar{\mu}^2 \ll \Pi_{T/L}$. Using (53), (55), and (23), we obtain the following representation:

$$\begin{aligned}\Sigma_{ar}^A(P) &= \frac{N_c^2 - 1}{2N_c} g^2 \int \frac{d^4 Q}{(2\pi)^4} \gamma^\mu \frac{i(\not{P} - \not{Q})}{(P - Q)^2 + i\epsilon(p_0 - q_0)} \gamma^\nu \left(\frac{1}{2} + f_g(q_0) \right) \\ &\times 2i \text{Im} \left[\frac{Q^2 q^2}{(Q^2 - \Pi_T)(q^2 Q^2 (q_0^3 - q_3^2) - Q^2 q_3^2 \Pi_T - q_0^2 q_\perp^2 \Pi_L)} \right] A_{\mu\nu} \bar{\mu}.\end{aligned} \quad (60)$$

As reasoned above, only spacelike Q in the spectral function contributes to the damping rate. In this case, it corresponds to the Landau damping cut, from which we obtain

$$\begin{aligned}\text{Re} \Sigma_{ar}^A(P) &= \frac{N_c^2 - 1}{2N_c} g^2 \int \frac{d^3 q}{(2\pi)^4} \frac{\pi T}{2p q_0} \left(\frac{2i\bar{\mu}}{q^2} \right) (q_0^2 f_1 + q_0 f_2) \\ &\times 2i \text{Im} \left[\frac{Q^2 q^2}{(Q^2 - \Pi_T)(q^2 Q^2 (q_0^3 - q_3^2) - Q^2 q_3^2 \Pi_T - q_0^2 q_\perp^2 \Pi_L)} \right] \Big|_{q_0 = \hat{\mathbf{p}} \cdot \mathbf{q}}.\end{aligned} \quad (61)$$

We can further simplify the integral by noting that $\text{Im} \left[\frac{Q^2 q^2}{(Q^2 - \Pi_T)(q^2 Q^2 (q_0^3 - q_3^2) - Q^2 q_3^2 \Pi_T - q_0^2 q_\perp^2 \Pi_L)} \right]$ is odd in q_0 , thus also odd under $\mathbf{q} \rightarrow -\mathbf{q}$. To have an integrand even under $\mathbf{q} \rightarrow -\mathbf{q}$, we can just keep the following terms in f_1 and f_2 :

$$f_1 = -q^2 \gamma^5 \gamma^3, \quad f_2 = q_3 q^2 \gamma^5 \gamma^0. \quad (62)$$

We then parameterize the quark self-energy as

$$\text{Re} \Sigma_{ar}^A(P) \equiv \frac{N_c^2 - 1}{2N_c} g^2 \int \frac{dq}{(2\pi)^4} \frac{\pi T \bar{\mu}}{p} (h_1 \gamma^5 \gamma^3 + h_2 \gamma^5 \gamma^0). \quad (63)$$

By rotational invariance, h_1 and h_2 are even and odd functions of \hat{p}_3 , respectively. Their precise forms can only be obtained numerically. We use the following parameterization of q :

$$\begin{aligned}\mathbf{q} &= q \cos \alpha \hat{p} + q \sin \alpha \cos \beta \frac{\hat{b} - \cos \gamma \hat{p}}{\sin \gamma} \\ &+ q \sin \alpha \sin \beta \frac{\hat{b} \times \hat{p}}{\sin \gamma}.\end{aligned} \quad (64)$$

We have chosen \hat{p} as the z axis and the plane spanned by \hat{p} and \hat{b} as the z - x plane. γ denotes the angle between \hat{p} and \hat{b}

with $\cos\gamma = \hat{p} \cdot \hat{b}$. We have then $\hat{p} \cdot \hat{q} = \cos\alpha$ and $d^3q = q^2 dq d\cos\alpha d\beta$. The angular integration is performed numerically to obtain $h_{1,2}$.

The q dependence is of particular interest. It has been shown that the dynamical screening crucial for the damping rate is the same as the case without magnetic field in the IR limit [56]. It follows that the damping rate from symmetric contributions contains logarithmic divergence [58]. One may expect similar logarithmic divergence in the splitting of damping rate from antisymmetric contributions. It turns out that this is not the case. Figure 2 shows the q dependence of $h_{1,2}$ for a generic $\cos\gamma$. Both h_1 and h_2 are IR safe. In the UV h_2 decays more slowly than h_1 . Let us define the q -integrated quantities as

$$\text{Re}\Sigma_{ar}^A(P) = H_1\gamma^5\gamma^3 - \epsilon(p_3)H_2\gamma^5\gamma^0, \quad (65)$$

with

$$\begin{aligned} H_1 &= \frac{N_c^2 - 1}{2N_c} g^2 \frac{\pi T \bar{\mu}}{(2\pi)^4 p} \int_0^{q_{UV}} dq h_1, \\ H_2 &= \frac{N_c^2 - 1}{2N_c} g^2 \frac{\pi T \bar{\mu}}{(2\pi)^4 p} \int_0^{q_{UV}} dq |h_2|. \end{aligned} \quad (66)$$

We have taken into account the signs of h_1 and h_2 (note that the latter is an odd function of \hat{p}_3) such that both H_1 and H_2 are positive. This leads to the following dispersions:

$$\begin{aligned} L: p_0 &\simeq p - \frac{ip_3 H_1}{p} + i\text{sgn}(p_3)H_2, \\ R: p_0 &\simeq p + \frac{ip_3 H_1}{p} - i\text{sgn}(p_3)H_2, \end{aligned} \quad (67)$$

with the following damping rate:

$$\begin{aligned} \Gamma_L &\simeq -\text{sgn}(p_3) \left(H_2 - \frac{|p_3| H_1}{p} \right), \\ \Gamma_R &\simeq \text{sgn}(p_3) \left(H_2 - \frac{|p_3| H_1}{p} \right). \end{aligned} \quad (68)$$

To determine which mode is unstable, we need to compare H_2 with $\frac{|p_3| H_1}{p}$, which depends on the choice of q_{UV} . In the magnetized plasma limit with the cut contribution, we may estimate $q \sim q_0 \sim \tau_R^{-1} \sim g^4 T$, thus $q_{UV} \sim g^4 T \ll m$. From Fig. 2, we see h_1 dominates over h_2 in the range of integration schematically indicated by the yellow band, so we may consider the H_1 term in (68) only. It follows that (68) has the same structure as (43) so that the previous reasoning applies: the right-handed mode with $p_3 > 0$ and left-handed mode with $p_3 < 0$ are amplified with respect to their chiral partners. This is just the amplification of the mode with a positive spin component along the magnetic field, which provides a mechanism to polarize the probe quark by the QGP paramagnet.

We are ready to propose the following picture for polarization dynamics in heavy ion collisions: the initial strong magnetic field first polarizes the spin of light quarks in the QGP. At not very high energy, the QGP carries finite baryon density. Because of the mismatch of charges of up and down quarks, the medium is also electrically charged and thus can be treated as a magnet. We have analyzed the high density or low temperature limit and magnetized plasma limit. In both cases, the QGP behaves as a paramagnet. The initial magnetic field decays quickly so it cannot affect the strange quarks produced in the late stage of heavy ion collisions. Nevertheless, the spin polarized charged QGP serves as a paramagnet, which can efficiently polarize the strange quarks. This is realized through the splitting in the damping rates for quarks with opposite spin component along the magnetic field. Interestingly, this case leads to a splitting $\Delta\Gamma \sim \frac{g^4 T \mu}{p}$, which is parametrically larger than the high density case with $\Delta\Gamma \sim \frac{g^2 T q_{UV}^2}{\bar{\mu} p} \sim \frac{g^6 T \mu}{p}$.

Finally, let us comment on two simplifications made in our analysis. The first one is the LLL approximation. For a realistic magnetic field produced in heavy ion collisions, higher Landau level (hLL) contribution might not be negligible. Indeed, interesting phenomenological consequences have been discussed from inter-Landau level transitions [59–61]. How do they affect our results? Cutting the diagram in Fig. 1, we easily see that the self-energy of the probe quark comes from scattering with either quarks in the LLL states or gluons. The dominance of either of them corresponds to the low and high density limits, respectively. For the antisymmetric part of self-energy leading to the splitting, we need at least one scattering with LLL states. It is crucial that the LLL states are spin polarized. The splitting in damping rates for opposite spin states seems to imply that it is the spin of the LLL states that is transferred to the counterpart of the probe fermions.⁵ If this were true, we would expect no qualitative change from hLL contributions, because hLL states are twofold degenerate with opposite spins and their contributions would cancel in the splitting.

The second simplification is the neglect of quark mass, which is not necessarily small for strange quarks as compared to temperature. One may ask, when does our picture break down? For massive probe quarks, the right- and left-handed components can convert to each other on timescales of axial charge relaxation. The timescale has been estimated as $\tau_m \sim \frac{T}{m^2 g^2}$ [62]. If the relaxation timescale is much longer than the splitting timescale $\tau_{\text{split}} \sim \frac{1}{\Delta\Gamma}$, the polarization mechanism we propose is still effective. The condition corresponds to $\frac{T}{m^2 g^2} \gg \frac{p}{g^6 T \mu}$ in the high density limit and $\frac{T}{m^2 g^2} \gg \frac{p}{g^4 T \mu}$ in the low density limit. If the

⁵Note again the spin is entirely canceled by the orbital angular momentum in the LLL approximation.

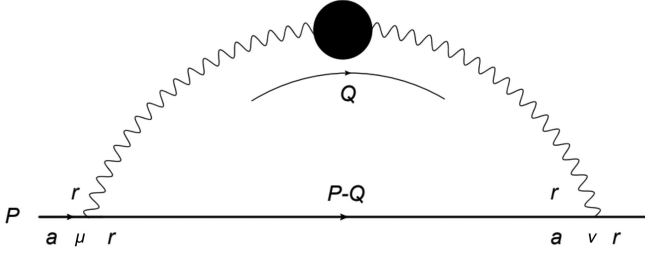


FIG. 1. One-loop fermion self-energy Σ_{ar} . Black solid circle represents the resummed photon propagator and the thick line indicates the probe fermion. The other diagram can be obtained by exchanging the ra labeling of the photon and probe fermion in the loop. Its contribution does not give rise to damping because the probe fermion is not thermally populated.

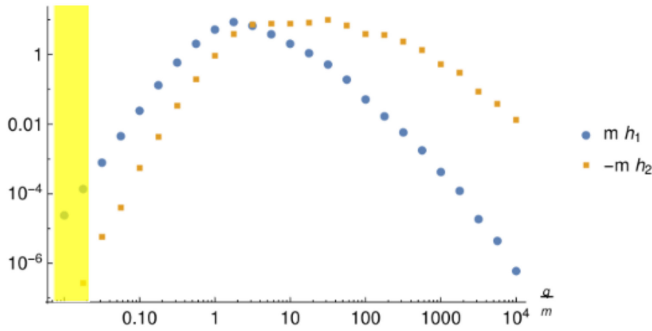


FIG. 2. q dependence of h_1 (disk) and h_2 (square) for $\hat{p} \cdot \hat{b} = \cos \gamma = \frac{1}{3}$. Both are finite in the IR and UV. The shape of the q dependence remains qualitatively the same for a wide range of $\hat{p} \cdot \hat{b}$. With $q_{UV} \ll m$, the integration range is schematically indicated by the yellow band. It follows that the integration of h_1 dominates the counterpart of h_2 .

relaxation time is much shorter than the splitting timescale instead, the polarization will be washed out.

V. CONCLUSION AND OUTLOOK

We have considered self-energies of photons/gluons in a charged magnetized medium in a strong magnetic field limit. Finite charge density of the medium induces an antisymmetric component in the self-energies. We have found the

antisymmetric component leads to splitting of damping rates for probe chiral fermions/quarks with opposite spin component along the magnetic field. We have analyzed the high and low density limits, finding the medium behaves like a paramagnet in both cases. Applying the results to heavy ion collisions, we propose the QGP consisting of light quarks can be analogous to a paramagnet due to the interplay of finite magnetic field and baryon density. After decay of initial magnetic field, the paramagnet can continue to polarize the strange quarks produced at late stage of heavy ion collisions. This provides a mechanism to effectively extend the lifetime of the magnetic field other than the electric conductivity.

Several extensions of this work can be considered: we have considered the strong magnetic field limit with the LLL approximation. We have argued the mechanism for polarization dynamics remains qualitatively the same based on the assumption that only the spin of the Landau level states matters for the polarization dynamics. It is desirable to confirm the picture in the weak field limit, where the spin and orbital angular momentum do not cancel each other. It is more interesting to consider the scenario with vorticity. Unlike the magnetized medium, the vortical medium carries mostly orbital angular momentum. It is known that an antisymmetric component exists in self-energy for gluons in neutral vortical QGP [63]. It is expected to lead to splitting of damping rates for different spin states, which leads to the polarization mechanism through spin-orbit coupling. We leave these for future studies.

ACKNOWLEDGMENTS

We are grateful to Koichi Hattori, Aihong Tang, and Pengfei Zhuang for helpful discussions. This work is in part supported by NSFC under Grants No. 12075328 and No. 11735007.

APPENDIX: EVALUATION OF THE PROBE FERMION SELF-ENERGY

In this appendix, we evaluate the probe fermion self-energy which is necessary to determine the damping rate in the main text. Let us start from the antisymmetric contribution of (36),

$$\begin{aligned}
 \Sigma_{ar}^A(P) &= -\frac{ie^2 T}{(2\pi)^3 \tilde{\mu}} \int \frac{d^3 q}{q^2} \frac{f_1}{\mathbf{p} \cdot \mathbf{q} + i\epsilon p_0} \\
 &= -\frac{ie^2 T \gamma^5 \gamma^3}{(2\pi)^3 \tilde{\mu}} \int \frac{d^3 q}{q^2} \frac{p_1 q_1 + p_2 q_2}{\mathbf{p} \cdot \mathbf{q} + i\epsilon p_0} + \frac{ie^2 T p_3 \gamma^5}{(2\pi)^3 \tilde{\mu}} \int \frac{d^3 q}{q^2} \frac{q_1 \gamma^1 + q_2 \gamma^2}{\mathbf{p} \cdot \mathbf{q} + i\epsilon p_0} + \frac{ie^2 T \gamma^5 \gamma^3}{(2\pi)^3 \tilde{\mu}} \int \frac{d^3 q}{\mathbf{p} \cdot \mathbf{q} + i\epsilon p_0} \\
 &= \frac{ie^2 T \gamma^5 \gamma^3}{(2\pi)^3 \tilde{\mu}} \int q_{\perp} dq_{\perp} d\phi \int \frac{dq_3}{p_{\perp} q_{\perp} \cos \phi + p_3 q_3 + i\epsilon p_0} \\
 &\quad - \frac{ie^2 T \gamma^5 \gamma^3}{(2\pi)^3 \tilde{\mu}} p_{\perp} \int q_{\perp}^2 \cos \phi dq_{\perp} d\phi \int \frac{dq_3}{(q_{\perp}^2 + q_3^2)(p_{\perp} q_{\perp} \cos \phi + p_3 q_3 + i\epsilon p_0)} \\
 &\quad + \frac{ie^2 T p_3 \gamma^5}{(2\pi)^3 \tilde{\mu}} \int q_{\perp} (\mathbf{q}_{\perp} \cdot \boldsymbol{\gamma}_{\perp}) dq_{\perp} d\phi \int \frac{dq_3}{(q_{\perp}^2 + q_3^2)(p_{\perp} q_{\perp} \cos \phi + p_3 q_3 + i\epsilon p_0)}, \tag{A1}
 \end{aligned}$$

with

$$\mathbf{q}_\perp \cdot \boldsymbol{\gamma}_\perp = \frac{q_\perp}{p_\perp} ((p_1 \cos \phi - p_2 \sin \phi)\gamma^1 + (p_1 \sin \phi + p_2 \cos \phi)\gamma^2). \quad (\text{A2})$$

ϕ is the angle between \mathbf{p}_\perp and \mathbf{q}_\perp . We have used the cylindrical coordinates to calculate this integral.

Next, we will use the residue theorem to calculate the above integral. The sign of p_0 and p_3 will affect the integral result. Therefore, we consider the following two cases that are related to our study: one case is $p_0 > 0$ and $p_3 > 0$, the other case is $p_0 > 0$ and $p_3 < 0$.

As for the first case ($p_0 > 0$ and $p_3 > 0$), the integral results of q_3 are

$$\int \frac{dq_3}{p_\perp q_\perp \cos \phi + p_3 q_3 + i\epsilon p_0} = -\frac{i\pi}{p_3}, \quad \int \frac{dq_3}{(q_\perp^2 + q_3^2)(p_\perp q_\perp \cos \phi + p_3 q_3 + i\epsilon p_0)} = \frac{\pi}{q_\perp^2 (ip_3 + p_\perp \cos \phi)}. \quad (\text{A3})$$

Then, (A1) becomes

$$\begin{aligned} \Sigma_{ar}^A(P) &= \frac{ie^2 T p_3 q_{UV}}{8\pi^2 \tilde{\mu} p_\perp} \gamma^5 \int d\phi \frac{(p_1 \cos \phi - p_2 \sin \phi)\gamma^1 + (p_1 \sin \phi + p_2 \cos \phi)\gamma^2}{ip_3 + p_\perp \cos \phi} \\ &\quad - \frac{ie^2 T p_\perp q_{UV}}{8\pi^2 \tilde{\mu}} \gamma^5 \gamma^3 \int \frac{d\phi \cos \phi}{ip_3 + p_\perp \cos \phi} + \frac{e^2 T q_{UV}^2}{8\pi \tilde{\mu} p_3} \gamma^5 \gamma^3. \end{aligned} \quad (\text{A4})$$

Let $z = e^{i\phi}$, $\cos \phi = \frac{z^2+1}{2z}$, and $\sin \phi = \frac{z^2-1}{2z}$, then we can obtain

$$\begin{aligned} \Sigma_{ar}^A(P) &= \frac{e^2 T p_3 q_{UV}}{8\pi^2 \tilde{\mu} p_\perp} \gamma^5 \oint_{|z|=1} \frac{dz}{z} \left(\frac{(z^2+1)(p_1 \gamma^1 + p_2 \gamma^2)}{p_\perp (z^2+1) + 2izp_3} + \frac{(z^2-1)(p_1 \gamma^2 - p_2 \gamma^1)}{i(p_\perp (z^2+1) + 2izp_3)} \right) \\ &\quad - \frac{e^2 T p_\perp q_{UV}}{8\pi^2 \tilde{\mu}} \gamma^5 \gamma^3 \oint_{|z|=1} \frac{dz}{z} \frac{z^2+1}{p_\perp (z^2+1) + 2izp_3} + \frac{e^2 T q_{UV}^2}{8\pi \tilde{\mu} p_3} \gamma^5 \gamma^3. \end{aligned} \quad (\text{A5})$$

The consequences of $\oint dz$ are

$$\oint_{|z|=1} \frac{dz}{z} \frac{(z^2+1)}{p_\perp (z^2+1) + 2izp_3} = \frac{2\pi i}{p_\perp} \left(1 - \frac{p_3}{p} \right), \quad \oint_{|z|=1} \frac{dz}{z} \frac{(z^2-1)}{p_\perp (z^2+1) + 2izp_3} = 0. \quad (\text{A6})$$

Substituting (A6) into (A5), we can get the final result

$$\Sigma_{ar}^A(P) = -\frac{ie^2 T q_{UV}}{4\pi \tilde{\mu}} \left(1 - \frac{p_3}{p} \right) \left(\gamma^5 \gamma^3 - \frac{p_3}{p_\perp^2} \gamma^5 (p_1 \gamma^1 + p_2 \gamma^2) \right) + \frac{e^2 T q_{UV}^2}{8\pi \tilde{\mu} p_3} \gamma^5 \gamma^3. \quad (\text{A7})$$

We can use a similar method to calculate the second case ($p_0 > 0$ and $p_3 < 0$). The integral results of q_3 are

$$\int \frac{dq_3}{p_\perp q_\perp \cos \phi + p_3 q_3 + i\epsilon p_0} = \frac{i\pi}{p_3}, \quad \int \frac{dq_3}{(q_\perp^2 + q_3^2)(p_\perp q_\perp \cos \phi + p_3 q_3 + i\epsilon p_0)} = \frac{\pi}{q_\perp^2 (p_\perp \cos \phi - ip_3)}. \quad (\text{A8})$$

Then, (A1) becomes

$$\begin{aligned} \Sigma_{ar}^A(P) &= \frac{ie^2 T p_3 q_{UV}}{8\pi^2 \tilde{\mu} p_\perp} \gamma^5 \int d\phi \frac{(p_1 \cos \phi - p_2 \sin \phi)\gamma^1 + (p_1 \sin \phi + p_2 \cos \phi)\gamma^2}{p_\perp \cos \phi - ip_3} \\ &\quad - \frac{ie^2 T p_\perp q_{UV}}{8\pi^2 \tilde{\mu}} \gamma^5 \gamma^3 \int \frac{d\phi \cos \phi}{p_\perp \cos \phi - ip_3} - \frac{e^2 T q_{UV}^2}{8\pi \tilde{\mu} p_3} \gamma^5 \gamma^3. \end{aligned} \quad (\text{A9})$$

We substitute $z = e^{i\phi}$, $\cos \phi = \frac{z^2+1}{2z}$, and $\sin \phi = \frac{z^2-1}{2z}$ into the above equation,

$$\begin{aligned} \Sigma_{ar}^A(P) = & \frac{e^2 T p_3 q_{UV}}{8\pi^2 \tilde{\mu} p_\perp} \gamma^5 \oint_{|z|=1} \frac{dz}{z} \left(\frac{(z^2+1)(p_1 \gamma^1 + p_2 \gamma^2)}{p_\perp(z^2+1) - 2izp_3} + \frac{(z^2-1)(p_1 \gamma^2 - p_2 \gamma^1)}{i(p_\perp(z^2+1) - 2izp_3)} \right) \\ & - \frac{e^2 T p_\perp q_{UV}}{8\pi^2 \tilde{\mu}} \gamma^5 \gamma^3 \oint_{|z|=1} \frac{dz}{z} \frac{z^2+1}{p_\perp(z^2+1) - 2izp_3} - \frac{e^2 T q_{UV}^2}{8\pi \tilde{\mu} p_3} \gamma^5 \gamma^3. \end{aligned} \quad (A10)$$

The consequences of $\oint dz$ are

$$\oint_{|z|=1} \frac{dz}{z} \frac{z^2+1}{p_\perp(z^2+1) - 2izp_3} = \frac{2\pi i}{p_\perp} \left(1 + \frac{p_3}{p} \right), \quad \oint_{|z|=1} \frac{dz}{z} \frac{z^2-1}{(p_\perp(z^2+1) - 2izp_3)} = 0. \quad (A11)$$

Eventually, we get

$$\Sigma_{ar}^A(P) = -\frac{ie^2 T q_{UV}}{4\pi \tilde{\mu}} \left(1 + \frac{p_3}{p} \right) \left(\gamma^5 \gamma^3 - \frac{p_3}{p_\perp^2} \gamma^5 (p_1 \gamma^1 + p_2 \gamma^2) \right) - \frac{e^2 T q_{UV}^2}{8\pi \tilde{\mu} p_3} \gamma^5 \gamma^3. \quad (A12)$$

Combining (A7) and (A12), we can get back to the result of (38).

Let us turn to the symmetric contribution. We start from the following expression:

$$\Sigma_{ar}^S(P) = \frac{e^2}{(2\pi)^3} \int \frac{d^4 Q \text{sgn}(q_0)}{(P-Q)^2 + i\epsilon(p_0 - q_0)} \left(\frac{1}{2} + f_\gamma(q_0) \right) \left(\frac{\delta(q_0^2 - x_1^2)}{q_0^2 - x_2^2} + \frac{\delta(q_0^2 - x_2^2)}{q_0^2 - x_1^2} \right) \gamma^\mu (\mathbf{P} - \mathbf{Q}) \gamma^\nu S_{\mu\nu}(Q), \quad (A13)$$

We first deal with $\gamma^\mu (\mathbf{P} - \mathbf{Q}) \gamma^\nu S_{\mu\nu}(Q)$. The following result is obtained by considering only $\sim q_0^0$:

$$\gamma^\mu (\mathbf{P} - \mathbf{Q}) \gamma^\nu S_{\mu\nu}(Q) = -2iq_3^2 \left(p_0 \gamma^0 + \mathbf{q} \cdot \boldsymbol{\gamma} - \frac{(\mathbf{q} \cdot \boldsymbol{\gamma})(\mathbf{p} \cdot \mathbf{q})}{q^2} \right). \quad (A14)$$

Then, (A13) can be written as

$$\Sigma_{ar}^S(P) = \frac{ie^2 T}{(2\pi)^3 \tilde{\mu}^2} \int \frac{q_3^2 \left(p_0 \gamma^0 + \mathbf{q} \cdot \boldsymbol{\gamma} - \frac{(\mathbf{q} \cdot \boldsymbol{\gamma})(\mathbf{p} \cdot \mathbf{q})}{q^2} \right)}{(\mathbf{p} \cdot \mathbf{q} + i\epsilon p_0)} d^3 q \int \frac{dq_0}{q_0} \delta \left(q_0^2 - \frac{q_3^2 q^2}{\tilde{\mu}^2} \right) \text{sgn}(q_0). \quad (A15)$$

We proceed with the integral of q_0 ,

$$\int \frac{dq_0}{q_0} \delta \left(q_0^2 - \frac{q_3^2 q^2}{\tilde{\mu}^2} \right) \text{sgn}(q_0) = \frac{\tilde{\mu}^2}{q_3^2 q^2}. \quad (A16)$$

By using (A16), we can simplify (A15) and obtain

$$\Sigma_{ar}^S(P) = \frac{ie^2 T}{(2\pi)^3} \int \frac{d^3 q}{q^2 (\mathbf{p} \cdot \mathbf{q} + i\epsilon p_0)} \left(p_0 \gamma^0 + \mathbf{q} \cdot \boldsymbol{\gamma} - \frac{(\mathbf{q} \cdot \boldsymbol{\gamma})(\mathbf{p} \cdot \mathbf{q})}{q^2} \right). \quad (A17)$$

In cylindrical coordinates, the above equation can be rewritten as

$$\begin{aligned}
\Sigma_{ar}^S(P) = & \frac{ie^2 T \gamma^0 p_0}{(2\pi)^3} \int q_{\perp} dq_{\perp} d\phi \int \frac{dq_3}{(q_{\perp}^2 + q_3^2)(p_{\perp} q_{\perp} \cos \phi + p_3 q_3 + i\epsilon p_0)} \\
& + \frac{ie^2 T}{(2\pi)^3} \int q_{\perp} (\mathbf{q}_{\perp} \cdot \boldsymbol{\gamma}_{\perp}) dq_{\perp} d\phi \int \frac{dq_3}{(q_{\perp}^2 + q_3^2)(p_{\perp} q_{\perp} \cos \phi + p_3 q_3 + i\epsilon p_0)} \\
& + \frac{ie^2 T \gamma^3}{(2\pi)^3} \int q_{\perp} dq_{\perp} d\phi \int \frac{q_3 dq_3}{(q_{\perp}^2 + q_3^2)(p_{\perp} q_{\perp} \cos \phi + p_3 q_3 + i\epsilon p_0)} \\
& - \frac{ie^2 T}{(2\pi)^3} \int q_{\perp} (\mathbf{q}_{\perp} \cdot \boldsymbol{\gamma}_{\perp}) (\mathbf{q}_{\perp} \cdot \mathbf{p}_{\perp}) dq_{\perp} d\phi \int \frac{dq_3}{(q_{\perp}^2 + q_3^2)^2 (p_{\perp} q_{\perp} \cos \phi + p_3 q_3 + i\epsilon p_0)} \\
& - \frac{ie^2 T p_3}{(2\pi)^3} \int q_{\perp} (\mathbf{q}_{\perp} \cdot \boldsymbol{\gamma}_{\perp}) dq_{\perp} d\phi \int \frac{q_3 dq_3}{(q_{\perp}^2 + q_3^2)^2 (p_{\perp} q_{\perp} \cos \phi + p_3 q_3 + i\epsilon p_0)} \\
& - \frac{ie^2 T \gamma_3}{(2\pi)^3} \int q_{\perp} (\mathbf{q}_{\perp} \cdot \mathbf{p}_{\perp}) dq_{\perp} d\phi \int \frac{q_3 dq_3}{(q_{\perp}^2 + q_3^2)^2 (p_{\perp} q_{\perp} \cos \phi + p_3 q_3 + i\epsilon p_0)} \\
& - \frac{ie^2 T \gamma_3 p_3}{(2\pi)^3} \int q_{\perp} dq_{\perp} d\phi \int \frac{q_3^2 dq_3}{(q_{\perp}^2 + q_3^2)^2 (p_{\perp} q_{\perp} \cos \phi + p_3 q_3 + i\epsilon p_0)}. \tag{A18}
\end{aligned}$$

We still consider two cases. As for the case of $p_0 > 0$ and $p_3 > 0$, the integral results of q_3 are

$$\begin{aligned}
& \int \frac{q_3 dq_3}{(q_{\perp}^2 + q_3^2)(p_{\perp} q_{\perp} \cos \phi + p_3 q_3 + i\epsilon p_0)} = \frac{i\pi}{q_{\perp}(ip_3 + p_{\perp} \cos \phi)}, \\
& \int \frac{dq_3}{(q_{\perp}^2 + q_3^2)^2 (p_{\perp} q_{\perp} \cos \phi + p_3 q_3 + i\epsilon p_0)} = \frac{\pi(2ip_3 + p_{\perp} \cos \phi)}{2q_{\perp}^4 (ip_3 + p_{\perp} \cos \phi)^2}, \\
& \int \frac{q_3 dq_3}{(q_{\perp}^2 + q_3^2)^2 (p_{\perp} q_{\perp} \cos \phi + p_3 q_3 + i\epsilon p_0)} = \frac{-p_3 \pi}{2q_{\perp}^3 (ip_3 + p_{\perp} \cos \phi)^2}, \\
& \int \frac{q_3^2 dq_3}{(q_{\perp}^2 + q_3^2)^2 (p_{\perp} q_{\perp} \cos \phi + p_3 q_3 + i\epsilon p_0)} = \frac{\pi p_{\perp} \cos \phi}{2q_{\perp}^2 (ip_3 + p_{\perp} \cos \phi)^2}. \tag{A19}
\end{aligned}$$

We plug (A19) into (A18) and calculate the integral of q_{\perp} to get the following result:

$$\begin{aligned}
\Sigma_{ar}^S(P) = & \frac{ie^2 T \gamma^0 p_0}{8\pi^2} \ln \frac{q_{UV}}{q_{IR}} \int \frac{d\phi}{ip_3 + p_{\perp} \cos \phi} - \frac{e^2 T \gamma^3 q_{UV}}{8\pi^2} \int \frac{d\phi}{ip_3 + p_{\perp} \cos \phi} \\
& + \frac{ie^2 T q_{UV}}{8\pi^2 p_{\perp}} \int \frac{d\phi}{ip_3 + p_{\perp} \cos \phi} (\cos \phi (\gamma^1 p_1 + \gamma^2 p_2) + \sin \phi (\gamma^2 p_1 - \gamma^1 p_2)) \\
& - \frac{ie^2 T}{16\pi^2} \ln \frac{q_{UV}}{q_{IR}} \int \frac{(2ip_3 + p_{\perp} \cos \phi) d\phi}{(ip_3 + p_{\perp} \cos \phi)^2} ((\cos \phi)^2 (\gamma^1 p_1 + \gamma^2 p_2) + \sin \phi \cos \phi (\gamma^2 p_1 - \gamma^1 p_2)) \\
& + \frac{ie^2 T p_3^2}{16\pi^2 p_{\perp}} \ln \frac{q_{UV}}{q_{IR}} \int \frac{d\phi}{(ip_3 + p_{\perp} \cos \phi)^2} (\cos \phi (\gamma^1 p_1 + \gamma^2 p_2) + \sin \phi (\gamma^2 p_1 - \gamma^1 p_2)). \tag{A20}
\end{aligned}$$

Then we can calculate the integral of ϕ and write

$$\begin{aligned}
& \int \frac{d\phi}{ip_3 + p_{\perp} \cos \phi} = \frac{-2i\pi}{p}, \\
& \int \frac{(\cos \phi (\gamma^1 p_1 + \gamma^2 p_2) + \sin \phi (\gamma^2 p_1 - \gamma^1 p_2)) d\phi}{ip_3 + p_{\perp} \cos \phi} = \frac{2\pi}{p_{\perp}} \left(1 - \frac{p_3}{p}\right) (p^1 \gamma_1 + p_2 \gamma^2), \\
& \int \frac{d\phi}{(ip_3 + p_{\perp} \cos \phi)^2} (\cos \phi (\gamma^1 p_1 + \gamma^2 p_2) + \sin \phi (\gamma^2 p_1 - \gamma^1 p_2)) = -2i\pi \frac{p_{\perp}}{p^3} (\gamma^1 p_1 + \gamma^2 p_2), \\
& \int \frac{(2ip_3 + p_{\perp} \cos \phi) d\phi}{(ip_3 + p_{\perp} \cos \phi)^2} ((\cos \phi)^2 (\gamma^1 p_1 + \gamma^2 p_2) + \sin \phi \cos \phi (\gamma^2 p_1 - \gamma^1 p_2)) = -2i\pi \frac{p_3^2}{p^3} (\gamma^1 p_1 + \gamma^2 p_2). \tag{A21}
\end{aligned}$$

Substituting (A21) into (A20), we can obtain

$$\Sigma_{ar}^S(P) = \frac{e^2 T \gamma^0 p_0}{4\pi p} \ln \frac{q_{UV}}{q_{IR}} + \frac{ie^2 T \gamma^3 q_{UV}}{4\pi^2 p} + \frac{ie^2 T q_{UV}}{4\pi p_{\perp}^2} \left(1 - \frac{p_3}{p}\right) (\gamma^1 p_1 + \gamma^2 p_2). \quad (\text{A22})$$

As for the another case of $p_0 > 0$ and $p_3 < 0$, the integral results of q_3 change into

$$\begin{aligned} \int \frac{q_3 dq_3}{(q_{\perp}^2 + q_3^2)(p_{\perp} q_{\perp} \cos \phi + p_3 q_3 + i\epsilon p_0)} &= \frac{-i\pi}{q_{\perp}(p_{\perp} \cos \phi - ip_3)}, \\ \int \frac{dq_3}{(q_{\perp}^2 + q_3^2)^2 (p_{\perp} q_{\perp} \cos \phi + p_3 q_3 + i\epsilon p_0)} &= \frac{\pi(p_{\perp} \cos \phi - 2ip_3)}{2q_{\perp}^4 (p_{\perp} \cos \phi - ip_3)^2}, \\ \int \frac{q_3 dq_3}{(q_{\perp}^2 + q_3^2)^2 (p_{\perp} q_{\perp} \cos \phi + p_3 q_3 + i\epsilon p_0)} &= \frac{-p_3 \pi}{2q_{\perp}^3 (p_{\perp} \cos \phi - ip_3)^2}, \\ \int \frac{q_3^2 dq_3}{(q_{\perp}^2 + q_3^2)^2 (p_{\perp} q_{\perp} \cos \phi + p_3 q_3 + i\epsilon p_0)} &= \frac{\pi p_{\perp} \cos \phi}{2q_{\perp}^2 (p_{\perp} \cos \phi - ip_3)^2}. \end{aligned} \quad (\text{A23})$$

After using the result of (A23), (A18) becomes

$$\begin{aligned} \Sigma_{ar}^S(P) &= \frac{ie^2 T \gamma^0 p_0}{8\pi^2} \ln \frac{q_{UV}}{q_{IR}} \int \frac{d\phi}{p_{\perp} \cos \phi - ip_3} + \frac{e^2 T \gamma^3 q_{UV}}{8\pi^2} \int \frac{d\phi}{p_{\perp} \cos \phi - ip_3} \\ &+ \frac{ie^2 T q_{UV}}{8\pi^2 p_{\perp}} \int \frac{d\phi}{p_{\perp} \cos \phi - ip_3} (\cos \phi (\gamma^1 p_1 + \gamma^2 p_2) + \sin \phi (\gamma^2 p_1 - \gamma^1 p_2)) \\ &- \frac{ie^2 T}{16\pi^2} \ln \frac{q_{UV}}{q_{IR}} \int \frac{(p_{\perp} \cos \phi - 2ip_3) d\phi}{(p_{\perp} \cos \phi - ip_3)^2} ((\cos \phi)^2 (\gamma^1 p_1 + \gamma^2 p_2) + \sin \phi \cos \phi (\gamma^2 p_1 - \gamma^1 p_2)) \\ &+ \frac{ie^2 T p_3^2}{16\pi^2 p_{\perp}} \ln \frac{q_{UV}}{q_{IR}} \int \frac{d\phi}{(p_{\perp} \cos \phi - ip_3)^2} (\cos \phi (\gamma^1 p_1 + \gamma^2 p_2) + \sin \phi (\gamma^2 p_1 - \gamma^1 p_2)). \end{aligned} \quad (\text{A24})$$

We take advantage of the same method as before to integrate ϕ to get the following result:

$$\begin{aligned} \int \frac{d\phi}{p_{\perp} \cos \phi - ip_3} &= \frac{-2i\pi}{p}, \\ \int \frac{(\cos \phi (\gamma^1 p_1 + \gamma^2 p_2) + \sin \phi (\gamma^2 p_1 - \gamma^1 p_2)) d\phi}{p_{\perp} \cos \phi - ip_3} &= \frac{2\pi}{p_{\perp}} \left(1 + \frac{p_3}{p}\right) (p^1 \gamma_1 + p_2 \gamma^2), \\ \int \frac{d\phi}{(p_{\perp} \cos \phi - ip_3)^2} (\cos \phi (\gamma^1 p_1 + \gamma^2 p_2) + \sin \phi (\gamma^2 p_1 - \gamma^1 p_2)) &= -2i\pi \frac{p_{\perp}}{p^3} (\gamma^1 p_1 + \gamma^2 p_2), \\ \int \frac{(p_{\perp} \cos \phi - 2ip_3) d\phi}{(p_{\perp} \cos \phi - ip_3)^2} ((\cos \phi)^2 (\gamma^1 p_1 + \gamma^2 p_2) + \sin \phi \cos \phi (\gamma^2 p_1 - \gamma^1 p_2)) &= -2i\pi \frac{p_3^2}{p^3} (\gamma^1 p_1 + \gamma^2 p_2). \end{aligned} \quad (\text{A25})$$

In the end, we can obtain

$$\Sigma_{ar}^S(P) = \frac{e^2 T \gamma^0 p_0}{4\pi p} \ln \frac{q_{UV}}{q_{IR}} - \frac{ie^2 T \gamma^3 q_{UV}}{4\pi^2 p} + \frac{ie^2 T q_{UV}}{4\pi p_{\perp}^2} \left(1 + \frac{p_3}{p}\right) (\gamma^1 p_1 + \gamma^2 p_2). \quad (\text{A26})$$

Combining (A22) and (A26), we can obtain the result of (40). Similarly, for the case where $p_0 < 0$, we do not elaborate further.

- [1] L. Adamczyk *et al.*, Global Λ hyperon polarization in nuclear collisions: Evidence for the most vortical fluid, *Nature (London)* **548**, 62 (2017).
- [2] Zuo-Tang Liang and Xin-Nian Wang, Globally polarized quark-gluon plasma in noncentral $A + A$ collisions, *Phys. Rev. Lett.* **94**, 102301 (2005); **96**, 039901(E) (2006).
- [3] F. Becattini and F. Piccinini, The ideal relativistic spinning gas: Polarization and spectra, *Ann. Phys. (Amsterdam)* **323**, 2452 (2008).
- [4] F. Becattini, V. Chandra, L. Del Zanna, and E. Grossi, Relativistic distribution function for particles with spin at local thermodynamical equilibrium, *Ann. Phys. (Amsterdam)* **338**, 32 (2013).
- [5] Ren-hong Fang, Long-gang Pang, Qun Wang, and Xin-nian Wang, Polarization of massive fermions in a vortical fluid, *Phys. Rev. C* **94**, 024904 (2016).
- [6] F. Becattini, Wojciech Florkowski, and Enrico Speranza, Spin tensor and its role in non-equilibrium thermodynamics, *Phys. Lett. B* **789**, 419 (2019).
- [7] Jian-Hua Gao and Shi-Zheng Yang, Revisit spin effects induced by thermal vorticity, *Chin. Phys. C* **48**, 053114 (2024).
- [8] I. Karpenko and F. Becattini, Study of Λ polarization in relativistic nuclear collisions at $\sqrt{s_{NN}} = 7.7\text{--}200$ GeV, *Eur. Phys. J. C* **77**, 213 (2017).
- [9] Yifeng Sun and Che Ming Ko, Λ hyperon polarization in relativistic heavy ion collisions from a chiral kinetic approach, *Phys. Rev. C* **96**, 024906 (2017).
- [10] Hui Li, Long-Gang Pang, Qun Wang, and Xiao-Liang Xia, Global Λ polarization in heavy-ion collisions from a transport model, *Phys. Rev. C* **96**, 054908 (2017).
- [11] De-Xian Wei, Wei-Tian Deng, and Xu-Guang Huang, Thermal vorticity and spin polarization in heavy-ion collisions, *Phys. Rev. C* **99**, 014905 (2019).
- [12] Yilong Xie, Dujuan Wang, and László P. Csernai, Global Λ polarization in high energy collisions, *Phys. Rev. C* **95**, 031901 (2017).
- [13] F. Becattini, I. Karpenko, M. Lisa, I. Upsal, and S. Voloshin, Global hyperon polarization at local thermodynamic equilibrium with vorticity, magnetic field and feed-down, *Phys. Rev. C* **95**, 054902 (2017).
- [14] Yu Guo, Shuzhe Shi, Shengqin Feng, and Jinfeng Liao, Magnetic field induced polarization difference between hyperons and anti-hyperons, *Phys. Lett. B* **798**, 134929 (2019).
- [15] Kun Xu, Fan Lin, Anping Huang, and Mei Huang, Λ/Λ^- polarization and splitting induced by rotation and magnetic field, *Phys. Rev. D* **106**, L071502 (2022).
- [16] L. P. Csernai, J. I. Kapusta, and T. Welle, Λ and $\bar{\Lambda}$ spin interaction with meson fields generated by the baryon current in high energy nuclear collisions, *Phys. Rev. C* **99**, 021901 (2019).
- [17] Ze-Fang Jiang, Xiang-Yu Wu, Shanshan Cao, and Ben-Wei Zhang, Directed flow and global polarization in Au + Au collisions across energies covered by the beam energy scan at RHIC, *Phys. Rev. C* **107**, 034904 (2023).
- [18] Victor E. Ambrus and M. N. Chernodub, Hyperon–anti-hyperon polarization asymmetry in relativistic heavy-ion collisions as an interplay between chiral and helical vortical effects, *Eur. Phys. J. C* **82**, 61 (2022).
- [19] L. McLerran and V. Skokov, Comments about the electromagnetic field in heavy-ion collisions, *Nucl. Phys.* **A929**, 184 (2014).
- [20] Hui Li, Xin-li Sheng, and Qun Wang, Electromagnetic fields with electric and chiral magnetic conductivities in heavy ion collisions, *Phys. Rev. C* **94**, 044903 (2016).
- [21] Alessandro Amato, Gert Aarts, Chris Allton, Pietro Giudice, Simon Hands, and Jon-Ivar Skullerud, Electrical conductivity of the quark-gluon plasma across the deconfinement transition, *Phys. Rev. Lett.* **111**, 172001 (2013).
- [22] Gert Aarts, Chris Allton, Alessandro Amato, Pietro Giudice, Simon Hands, and Jon-Ivar Skullerud, Electrical conductivity and charge diffusion in thermal QCD from the lattice, *J. High Energy Phys.* **02** (2015) 186.
- [23] Bastian B. Brandt, Anthony Francis, Benjamin Jäger, and Harvey B. Meyer, Charge transport and vector meson dissociation across the thermal phase transition in lattice QCD with two light quark flavors, *Phys. Rev. D* **93**, 054510 (2016).
- [24] Heng-Tong Ding, Olaf Kaczmarek, and Florian Meyer, Thermal dilepton rates and electrical conductivity of the QGP from the lattice, *Phys. Rev. D* **94**, 034504 (2016).
- [25] Nikita Astrakhantsev, V. V. Braguta, Massimo D’Elia, A. Yu. Kotov, A. A. Nikolaev, and Francesco Sanfilippo, Lattice study of the electromagnetic conductivity of the quark-gluon plasma in an external magnetic field, *Phys. Rev. D* **102**, 054516 (2020).
- [26] Wei Li, Shu Lin, and Jiajie Mei, Conductivities of magnetic quark-gluon plasma at strong coupling, *Phys. Rev. D* **98**, 114014 (2018).
- [27] Kenji Fukushima and Akitoshi Okutsu, Electric conductivity with the magnetic field and the chiral anomaly in a holographic QCD model, *Phys. Rev. D* **105**, 054016 (2022).
- [28] Koichi Hattori and Daisuke Satow, Electrical conductivity of quark-gluon plasma in strong magnetic fields, *Phys. Rev. D* **94**, 114032 (2016).
- [29] Koichi Hattori, Shiyong Li, Daisuke Satow, and Ho-Ung Yee, Longitudinal conductivity in strong magnetic field in perturbative QCD: Complete leading order, *Phys. Rev. D* **95**, 076008 (2017).
- [30] Kenji Fukushima and Yoshimasa Hidaka, Resummation for the field-theoretical derivation of the negative magnetoresistance, *J. High Energy Phys.* **04** (2020) 162.
- [31] Kenji Fukushima and Yoshimasa Hidaka, Electric conductivity of hot and dense quark matter in a magnetic field with Landau level resummation via kinetic equations, *Phys. Rev. Lett.* **120**, 162301 (2018).
- [32] Shu Lin and Lixin Yang, Chiral kinetic theory from Landau level basis, *Phys. Rev. D* **101**, 034006 (2020).
- [33] Aritra Bandyopadhyay, Sabyasachi Ghosh, Ricardo L. S. Farias, Jayanta Dey, and Gastão Krein, Anisotropic electrical conductivity of magnetized hot quark matter, *Phys. Rev. D* **102**, 114015 (2020).
- [34] Li Yan and Xu-Guang Huang, Dynamical evolution of a magnetic field in the preequilibrium quark-gluon plasma, *Phys. Rev. D* **107**, 094028 (2023).
- [35] Hao-Hao Peng, Xin-Li Sheng, Shi Pu, and Qun Wang, Electric and magnetic conductivities in magnetized fermion systems, *Phys. Rev. D* **107**, 116006 (2023).

- [36] Kun Xu, Shuzhe Shi, Hui Zhang, Defu Hou, Jinfeng Liao, and Mei Huang, Extracting the magnitude of magnetic field at freeze-out in heavy-ion collisions, *Phys. Lett. B* **809**, 135706 (2020).
- [37] Koichi Hattori, Kazunori Itakura, and Sho Ozaki, Strong-field physics in QED and QCD: From fundamentals to applications, *Prog. Part. Nucl. Phys.* **133**, 104068 (2023).
- [38] G. S. Bali, F. Bruckmann, G. Endrödi, S. D. Katz, and A. Schäfer, The QCD equation of state in background magnetic fields, *J. High Energy Phys.* **08** (2014) 177.
- [39] Gunnar S. Bali, Gergely Endrödi, and Stefano Piemonte, Magnetic susceptibility of QCD matter and its decomposition from the lattice, *J. High Energy Phys.* **07** (2020) 183.
- [40] L. Levkova and C. DeTar, Quark-gluon plasma in an external magnetic field, *Phys. Rev. Lett.* **112**, 012002 (2014).
- [41] P. V. Buividovich, D. Smith, and L. von Smekal, Static magnetic susceptibility in finite-density $SU(2)$ lattice gauge theory, *Eur. Phys. J. A* **57**, 293 (2021).
- [42] Koichi Hattori and Kazunori Itakura, In-medium polarization tensor in strong magnetic fields (I): Magneto-birefringence at finite temperature and density, *Ann. Phys. (Amsterdam)* **446**, 169114 (2022).
- [43] Koichi Hattori and Kazunori Itakura, In-medium polarization tensor in strong magnetic fields (II): Axial Ward identity at finite temperature and density, *Ann. Phys. (Amsterdam)* **446**, 169115 (2022).
- [44] Electromagnetic waves in anisotropic media, *Electrodynamics of Continuous Media* (Second Edition), edited by L. D. Landau and E. M. Lifshitz, Course of Theoretical Physics, Vol. 8 (Pergamon, Amsterdam, 1984), Chap. XI, pp. 331–357.
- [45] Kuang-chao Chou, Zhao-bin Su, Bai-lin Hao, and Lu Yu, Equilibrium and nonequilibrium formalisms made unified, *Phys. Rep.* **118**, 1 (1985).
- [46] Kenji Fukushima, Magnetic-field induced screening effect and collective excitations, *Phys. Rev. D* **83**, 111501 (2011).
- [47] Han Gao, Zonglin Mo, and Shu Lin, Photon self-energy in a magnetized chiral plasma from kinetic theory, *Phys. Rev. D* **102**, 014011 (2020).
- [48] Shu Lin and Lixin Yang, Magneto-vortical effect in strong magnetic field, *J. High Energy Phys.* **06** (2021) 054.
- [49] Lixin Yang, Two-point functions from chiral kinetic theory in magnetized plasma, *Phys. Rev. D* **105**, 074039 (2022).
- [50] Dmitri E. Kharzeev and Ho-Ung Yee, Chiral magnetic wave, *Phys. Rev. D* **83**, 085007 (2011).
- [51] Juan Hernandez and Pavel Kovtun, Relativistic magneto-hydrodynamics, *J. High Energy Phys.* **05** (2017) 001.
- [52] Kenji Fukushima, Koichi Hattori, Ho-Ung Yee, and Yi Yin, Heavy quark diffusion in strong magnetic fields at weak coupling and implications for elliptic flow, *Phys. Rev. D* **93**, 074028 (2016).
- [53] Michel Le Bellac, *Thermal Field Theory*, Cambridge Monographs on Mathematical Physics (Cambridge University Press, Cambridge, England, 2011), p. 3.
- [54] E. V. Gorbar, V. A. Miransky, and I. A. Shovkovy, Chiral asymmetry of the Fermi surface in dense relativistic matter in a magnetic field, *Phys. Rev. C* **80**, 032801 (2009).
- [55] Jean-Paul Blaizot and Edmond Iancu, Lifetime of quasi-particles in hot QED plasmas, *Phys. Rev. Lett.* **76**, 3080 (1996).
- [56] Koichi Hattori and Daisuke Satow, Gluon spectrum in a quark-gluon plasma under strong magnetic fields, *Phys. Rev. D* **97**, 014023 (2018).
- [57] Yoshimasa Hidaka and Robert D. Pisarski, Hard thermal loops, to quadratic order, in the background of a spatial 't Hooft loop, *Phys. Rev. D* **80**, 036004 (2009); **102**, 059902 (E) (2020).
- [58] Eric Braaten and Markus H. Thoma, Energy loss of a heavy quark in the quark-gluon plasma, *Phys. Rev. D* **44**, R2625 (1991).
- [59] Xinyang Wang, Igor A. Shovkovy, Lang Yu, and Mei Huang, Ellipticity of photon emission from strongly magnetized hot QCD plasma, *Phys. Rev. D* **102**, 076010 (2020).
- [60] Xinyang Wang and Igor Shovkovy, Photon polarization tensor in a magnetized plasma: Absorptive part, *Phys. Rev. D* **104**, 056017 (2021).
- [61] Xinyang Wang and Igor Shovkovy, Polarization tensor of magnetized quark-gluon plasma at nonzero baryon density, *Eur. Phys. J. C* **81**, 901 (2021).
- [62] De-fu Hou and Shu Lin, Fluctuation and dissipation of axial charge from massive quarks, *Phys. Rev. D* **98**, 054014 (2018).
- [63] Defu Hou and Shu Lin, Polarization rotation of chiral fermions in vortical fluid, *Phys. Lett. B* **818**, 136386 (2021).